Detection and mapping of hydrocarbon deposits on Titan

Roger Clark, John Curchin, Jason Barnes, Ralf Jaumann, Larry Soderblom, Dale Cruikshank, Robert Brown, Sébastien Rodriguez, Jonathan Lunine, Katrin Stephan, et al.

Detection and mapping of hydrocarbon deposits on Titan

Roger N. Clark,[1] John M. Curchin,[1] Jason W. Barnes,[2] Ralf Jaumann,[3] Larry Soderblom,[4] Dale P. Cruikshank,[5] Robert H. Brown,[6] Sébastien Rodriguez,[7] Jonathan Lunine,[8] Katrin Stephan,[3] Todd M. Hoefen,[1] Stéphane Le Mouélic,[9] Christophe Sotin,[10] Kevin H. Baines,[10] Bonnie J. Buratti,[10] and Philip D. Nicholson[11]

Received 2 March 2009; revised 23 March 2010; accepted 26 April 2010; published 13 October 2010.

[1] We report the identification of compounds on Titan's surface by spatially resolved imaging spectroscopy methods through Titan's atmosphere, and set upper limits to other organic compounds. We present evidence for surface deposits of solid benzene (C_6H_6), solid and/or liquid ethane (C_2H_6), or methane (CH_4), and clouds of hydrogen cyanide (HCN) aerosols using diagnostic spectral features in data from the Cassini Visual and Infrared Mapping Spectrometer (VIMS). Cyanoacetylene (2-propynenitrile, IUPAC nomenclature, HC_3N) is indicated in spectra of some bright regions, but the spectral resolution of VIMS is insufficient to make a unique identification although it is a closer match to the feature previously attributed to CO_2. We identify benzene, an aromatic hydrocarbon, in larger abundances than expected by some models. Acetylene (C_2H_2), expected to be more abundant on Titan according to some models than benzene, is not detected. Solid acetonitrile (CH_3CN) or other nitriles might be candidates for matching other spectral features in some Titan spectra. An as yet unidentified absorption at 5.01-μm indicates that yet another compound exists on Titan's surface. We place upper limits for liquid methane and ethane in some locations on Titan and find local areas consistent with millimeter path lengths. Except for potential lakes in the southern and northern polar regions, most of Titan appears "dry." Finally, we find there is little evidence for exposed water ice on the surface. Water ice, if present, must be covered with organic compounds to the depth probed by 1–5-μm photons: a few millimeters to centimeters.

Citation: Clark, R. N., et al. (2010), Detection and mapping of hydrocarbon deposits on Titan, *J. Geophys. Res.*, *115*, E10005, doi:10.1029/2009JE003369.

1. Introduction

[2] The surface composition of Titan is still enshrouded in a cloud of mystery despite the initial flood of data from the Cassini spacecraft and the Huygens probe. While the composition of Titan's atmosphere is known [*Coustenis et al.*, 2003, 2006, 2007; *Coustenis*, 2005; *Flasar et al.*, 2005; *Teanby et al.*, 2009, and references therein], with most of the observed gases having been predicted using models of UV photolysis and reactions of atmospheric methane and nitrogen [*Yung and DeMore*, 1999; *Vuitton et al.*, 2008, and references therein], the many less volatile molecules that coat and/or make up the solid surface have yet to be identified. Tholins are the solid end products of photolysis and electron discharge experiments done in terrestrial laboratories with gases common in Titan's atmosphere and are one type of mixture of compounds theorized to exist on Titan [*Sagan et al.*, 1992]. Tables 1a and 1b list known compounds on Titan through 2009.

[3] The Cassini RADAR has provided the highest spatial resolution images of Titan's surface from Saturn orbit but is a mono-frequency system that provides compositional information only through the dielectric constant of the surface at its operating wavelength of 2.16 cm [*Elachi et al.*, 2005]. Only the Descent Imager-Spectral Radiometer, DISR, on the Huygens probe and VIMS from the Cassini Saturn orbiter have the capability to provide combined spectral plus spatial information about the surface [*Tomasko et al.*, 2005; *Schroeder and Keller*, 2008; *Sotin et al.*, 2005; *Barnes et al.*,

[1]U.S. Geological Survey, Denver Federal Center, Denver, Colorado, USA.
[2]Department of Physics, University of Idaho, Moscow, Idaho, USA.
[3]Institute of Space Sensor Technology and Planetary Exploration, German Aerospace Center, Berlin, Germany.
[4]U.S. Geological Survey, Flagstaff, Arizona, USA.
[5]Astrophysics Branch, NASA Ames Research Center, Moffett Field, California, USA.
[6]Lunar and Planetary Laboratory, Department of Planetary Sciences, University of Arizona, Tucson, Arizona, USA.
[7]Laboratoire AIM, Université Paris 7, CNRS UMR-7158, CEA-Saclay/DSM/IRFU/SAp, Gif-sur-Yvette, France.
[8]Department of Physics, University of Rome Tor Vergata, Rome, Italy.
[9]Laboratoire de Planétologie et Géodynamique, UMR 6112, Université de Nantes, CNRS, Nantes, France.
[10]Jet Propulsion Laboratory, Pasadena, California, USA.
[11]Department of Astronomy, Cornell University, Ithaca, New York, USA.

0148-0227/10/2009JE003369

Table 1a. Compounds Identified on Titan: Atmosphere[a]

Compound	Location and Abundance	Instrument, Group, and Year[b]
	Major and Minor Gases (in Decreasing Abundance)	
Nitrogen, N_2	95% near surface	HASI, Huygens; *Fulchignoni et al.* [2005]
	98+% in stratosphere	GCMS, Huygens; *Niemann et al.* [2005]
	~97% near 1000 km	INMS, Cassini; *Waite et al.* [2007]
Methane, CH_4	~5% near surface	GCMS, Huygens; *Niemann et al.* [2005]
	1.4% in stratosphere	GCMS, Huygens; *Niemann et al.* [2005]
	~2% above 1000 km	INMS, Cassini; *Waite et al.* [2005]
Hydrogen, H_2	~0.1% in lower atmosphere	GCMS, Huygens; *Niemann et al.* [2005]
	0.4% above 1000 km	INMS, Cassini; *Waite et al.* [2005]
Argon, Ar	43×10^{-6} in stratosphere (^{40}Ar)	GCMS, Huygens; *Niemann et al.* [2005]
	0.28×10^{-6} in stratosphere (^{36}Ar)	GCMS, Huygens; *Niemann et al.* [2005]
	Hydrocarbons[c] (in Decreasing Abundance)	
Ethane, C_2H_6	$10 - 20 \times 10^{-6}$ in stratosphere	CIRS, Cassini; *Coustenis et al.* [2007]
	$8 - 20 \times 10^{-6}$ near 1000 km	INMS, Cassini; *Waite et al.* [2007]
	120×10^{-6} above 1000 km	INMS, Cassini; *Waite et al.* [2005]
Monodeuterated Methane, CH_3D	$\sim 7.5 \times 10^{-6}$ in stratosphere	CIRS, Cassini, *Coustenis et al.* [2007]
Acetylene, C_2H_2	$3 - 4 \times 10^{-6}$ in stratosphere	CIRS, Cassini; *Coustenis et al.* [2007]
	$200 - 260 \times 10^{-6}$ near 1000 km	INMS, Cassini, *Waite et al.* [2007]
	$\sim 190 \times 10^{-6}$ above 1000 km	INMS, Cassini; *Waite et al.* [2005]
Propane, C_3H_8	$0.5 - 0.8 \times 10^{-6}$ in stratosphere	CIRS, Cassini; *Coustenis et al.* [2007]
	$<5 \times 10^{-6}$ above 1000 km	INMS, Cassini; *Waite et al.* [2005]
Ethylene, C_2H_4	$0.1 - 0.2 \times 10^{-6}$ in stratosphere	CIRS, Cassini; *Coustenis et al.* [2007]
	$680 - 1000 \times 10^{-6}$ near 1000km	INMS, Cassini; *Waite et al.* [2007]
	$200 - 500 \times 10^{-6}$ above 1000 km	INMS, Cassini; *Waite et al.* [2005]
Propene, C_3H_6 (propylene)	$1.5 - 4 \times 10^{-6}$ near 1000 km	INMS, Cassini; *Waite et al.* [2007]
2-Propyne, C_3H_4 (methylacetylene)	$5 - 20 \times 10^{-9}$ in stratosphere	CIRS, Cassini; *Coustenis et al.* [2007]
	40×10^{-9} in stratosphere	CIRS, Cassini, *Teanby et al.* [2009]
	$7 - 12 \times 10^{-6}$ near 1000 km	INMS, Cassini; *Waite et al.* [2007]
	4×10^{-6} above 1000 km	INMS, Cassini; *Waite et al.* [2005]
1,3-Butadiyne, C_4H_2 (diacetylene)	$1 - 15 \times 10^{-9}$ in stratosphere	CIRS, Cassini; *Coustenis et al.* [2007]
	40×10^{-9} in stratosphere	CIRS, Cassini, *Teanby et al.* [2009]
	$2 - 6 \times 10^{-6}$ near 1000 km	INMS, Cassini; *Waite et al.* [2007]
	0.5×10^{-6} above 1000 km	INMS, Cassini; *Waite et al.* [2005]
Benzene, C_6H_6	up to 3×10^{-9} in stratosphere;	CIRS, Cassini; *Coustenis et al.* [2007]
	$\sim 0.3 \times 10^{-9}$ everywhere else	
	$1 - 5 \times 10^{-6}$ near 1000 km	INMS, Cassini; *Waite et al.* [2007]
	$<5 \times 10^{-6}$ above 1000 km	INMS, Cassini; *Waite et al.* [2005]
Monodeuterated Acetylene, C_2HD	1.3×10^{-9} atmosphere average	CIRS, Cassini; *Coustenis et al.* [2008]
Toluene, $C_6H_5CH_3$ (methylbenzene)	$<1 \times 10^{-6}$ *inferred* near 1000 km	INMS, Cassini; *Waite et al.* [2007]
Naphthalene, $C_{10}H_8$	$<1 \times 10^{-6}$ *inferred* near 1000 km	CAPS IBS, Cassini; *Waite et al.* [2007]
	Nitriles[c] (in Decreasing Abundance)	
Hydrogen Cyanide, HCN	$50 - 800 \times 10^{-9}$ in stratosphere	CIRS, Cassini; *Coustenis et al.* [2007]
	$<5 \times 10^{-6}$ above 1000 km	INMS, Cassini; *Waite et al.* [2005]
Cyanoacetylene, HC_3N	$0.1 - 25 \times 10^{-9}$ in stratosphere	CIRS, Cassini; *Coustenis et al.* [2007]
	$<5 \times 10^{-6}$ near 1000 km	INMS, Cassini; *Waite et al.* [2007]
Acetonitrile, CH_3CN (methyl cyanide)	"a few ppb" in upper atmosphere	IRAM 30 meter; *Marten et al.* [2002]
Acrylonitrile, C_2H_3CN (ethyl cyanide)	$<2 \times 10^{-9}$ in stratosphere (estimate *inferred* from data)	IRAM 30 meter; *Marten et al.* [2002]

Table 1a. (continued)

Compound	Location and Abundance	Instrument, Group, and Year[b]
Cyanogen, C_2N_2	5×10^{-9} in stratosphere	INMS, Cassini; *Waite et al.* [2005]
	$2 - 6 \times 10^{-6}$ above 1000 km	INMS, Cassini; *Waite et al.* [2007]
	55×10^{-12} in stratosphere	CIRS, Cassini, *Teanby et al.* [2009]
Dicyanoacetylene, C_4N_2	0.4×10^{-9} *inferred* at 90 km	IRIS, Voyager; *Coustenis et al.* [1989]
Propionitrile, C_2H_5CN	$<2 \times 10^{-9}$ in stratosphere	IRAM 30 meter; *Marten et al.* [2002]
Cyanodiacetylene, HC_5CN	$<0.4 \times 10^{-9}$ in stratosphere	IRAM 30 meter; *Marten et al.* [2002]
	Oxidized Species and Others (in Decreasing Abundance)	
Carbon Monoxide, CO	$\sim 47 \times 10^{-6}$ in stratosphere	CIRS, Cassini; *DeKok et al.* [2007]
Carbon Dioxide, CO_2	$\sim 15 \times 10^{-9}$ in stratosphere	CIRS, Cassini; *DeKok et al.* [2007]
Water, H_2O	$<0.9 \times 10^{-9}$ in stratosphere	CIRS, Cassini; *DeKok et al.* [2007]
	8×10^{-9} near 1000 km	INMS, Cassini; *Waite et al.* [2007]
Ammonia, NH_3	trace component of haze aerosols	ACP, Cassini; *Israel et al.* [2005]

[a]Generalized Atmospheric Structure: Troposphere: 0 – 44 km, Tropopause at 70 K (~44 km); Stratosphere: 44 – 250 km, Stratopause at 186 K (~250 km); Mesosphere: 250 – 490 km, Mesopause at 152 K (~490 km); Ionosphere: 490 – 1100+ km. The "<" symbol, when used, indicates an upper limit in abundance for that species.

[b]HASI, Huygens Atmospheric Structure Instrument; GCMS, Gas Chromatograph and Mass Spectrometer aboard Huygens probe; INMS, Ion and Neutral Mass Spectrometer, one of three CAPS spectrometers aboard Cassini; CIRS, Composite Infrared Spectrometer aboard Cassini; IRAM, International 30 meter Radiotelescope in Spanish Sierra Nevada; IRIS, Infrared Interferometer Spectrometer and Radiometer aboard Voyager; ACP, Aerosol Collector and Pyrolyser aboard Huygens probe; CAPS, Cassini Plasma Spctrometer; IBS, Ion Beam Spectrometer, one of three CAPS spectrometers aboard Cassini.

[c]The ranges in abundance, particularly for the nitriles and complex hydrocarbons, reflect higher concentrations in the stratosphere during winter and lower stratospheric concentrations in the summer.

2005, 2007a; *McCord et al.*, 2006, 2008; *Brown et al.*, 2008; *Rodriguez et al.*, 2006, *Nelson et al.*, 2009; *Soderblom et al.*, 2009]. The DISR is limited in wavelength range out to 1.7 μm but obtained very high spatial resolution over a limited area; VIMS measures out to 5.1 μm and can cover large parts of the surface of Titan but at much more limited spatial resolution. Terrestrially synthesized tholins do not match the spectral slope in data from the Huygens DISR [*Tomasko et al.*, 2005; *Schroeder and Keller*, 2008] or Cassini VIMS [*McCord et al.*, 2006]. The DISR spectra of Titan's surface show a blue spectral slope from 1 to 1.6 μm that is distinctly "un-tholin" like and show what qualitatively appears to be a water-ice absorption, but the complete H_2O feature was not covered by the spectrometer [*Tomasko et al.*, 2005; *Schroeder and Keller*, 2008] and Schroeder and Keller concluded the absorption did not match water ice. Also, the 1.25-μm H_2O absorption was not observed even though expected in the models presented by *Tomasko et al.* [2005] and *Schroeder and Keller* [2008]. In situ analyses have detected methane, ethane, and tentatively identified cyanogen, benzene, and carbon dioxide on the surface from the Huygens GCMS [*Niemann et al.*, 2005]. Ammonia and hydrogen cyanide were the main pyrolysis products of the aerosols measured by the Huygens in situ pyrolysis experiment during its descent [*Israel et al.*, 2005] and those aerosols could rain down to the surface, but pyrolysis products are not necessarily compounds in the aerosols. Higher in Titan's thermosphere, benzene was first detected in the stratosphere of Titan by ISO and CIRS [*Coustenis et al.*, 2003, 2007], and the Cassini Ion and Neutral Mass Spectrometer (INMS) instrument has detected high abundances of benzene along with toluene [*Waite et al.*, 2007] above 900 km. Toluene is an interesting molecule after benzene because toluene consists of a benzene ring with a methyl functional group, $-CH_3$, replacing one of the hydrogen atoms attached to the benzene ring, thus it is a possible larger organic molecule that may be compatible with observed VIMS surface spectra.

[4] We report the detection of distinct new absorption features seen through the 2.7 and 5-μm spectral windows in Titan's atmosphere and discuss their significance. The spectral properties of Titan from Cassini VIMS [*Brown et al.*, 2004] are well documented [*Sotin et al.*, 2005; *McCord et al.*, 2006, 2008; *Barnes et al.*, 2005]. Other windows (Figure 1) through which Titan's surface can be observed include those near 1.08, 1.28, 1.58, 2.01, 2.67, and 2.78 μm, but the 5-μm window is the widest and least affected by aerosol scattering [*Soderblom et al.*, 2009; *Sotin et al.*, 2005; *McCord et al.*, 2006; *Barnes et al.*, 2005].

2. Titan Atmospheric Transmittance

[5] As noted above, Titan is enshrouded in a haze that scatters most visible light from the surface and strong methane absorption blocking most of the near-infrared reflected solar spectral range, leaving only a few spectral windows through which to view the surface. Spectral windows where VIMS can detect the surface and show geologic patterns are illustrated in Figures 1 and 2. The windows at longer wavelengths provide a view with less scattering from atmospheric aerosols, as illustrated by 2 solar occultations observed by VIMS (Figures 3a, 3b, and 3c).

[6] Surface geology is apparent in VIMS data in the 2.7-μm window spanning from about 2.65 to 2.93 μm (VIMS channels 204 to 221). Surface geology is also apparent in the 5-μm

Table 1b. Compounds Identified on Titan: Surface[a]

Compound	Location Including Spectral Basis	Methods of Detection Including Author's "Confidence"[b]	Group and Year	Comments
		Major Hydrocarbons and Nitrile Condensates		
Methane, CH_4	Huygens Landing Site	GCMS (firm)	*Niemann et al.* [2005]	
	Select locations in 'dark' terrain	VIMS (probable, from absorption feature.)	This study	
Ethane, C_2H_6	Huygens Landing Site	GCMS (firm)	*Niemann et al.* [2005]	
	Ontario Lacus	VIMS (firm)	*Brown et al.* [2008]	
	Select locations in 'dark' terrain	VIMS (probable, from absorption feature.)	This study	
Benzene, C_6H_6	Huygens Landing Site	GCMS (tentative)	*Niemann et al.* [2005]	
	Select locations in 'dark' terrain, especially Fensal/Aztlan	VIMS (definite, from absorption feature.)	This study	
Cyanoacetylene, HC_3N	Select locations in 'bright' terrain	VIMS (possible)	This study	Note absorption feature not resolved.
Toluene, C_7H_8	Select locations in 'dark' terrain	VIMS (possible but not definitive)	This study	
Cyanogen, C_2N_2	Huygens Landing Site	GCMS (tentative)	*Niemann et al.* [2005]	
Acetonitrile, CH_3CN	Select locations in 'dark' terrain	VIMS (possible but not definitive)	This study	
		Oxidized and Other Species, including Unidentified Compounds		
Water, H_2O	Extensively exposed	UKIRT and IRTF	*Griffith et al.* [2003]	Features characteristic of water ice in spectral windows. Note inferred by spectral slope over Titan windows, not definitive.
	Disk-averaged surface spectra	ISO	*Coustenis et al.* [2006]	Spectra in near IR windows compatible with water ice. Note inferred by spectral slope over Titan windows, not definitive.
	~25% leading hemisphere; 12 – 15% trailing hemisphere	ESO – ISAAC	*Lellouch et al.* [2004]	Indicated from modelling of ensemble of inferred suface albedos. Note inferred by spectral slope over Titan windows, not definitive.
	Huygens Landing Site	DISR (inconclusive)	*Tomasko et al.* [2005]	
	Huygens Landing Site	VIMS, Cassini	*Rodriguez et al.* [2006]	1 of 7 units 'enriched', based on 'relative absorption signatures at 1.59 μm and 2.03 μm.' Note inferred by spectral slope over Titan windows, not definitive.
	Huygens Landing Site	DISR recalibrated	*Schroder and Keller* [2008]	'Inconclusive', based on near IR spectral slopes, and lack of 1.25-μm absorption.
	'Dark features', eg. Adiri, Quivira where $\kappa \sim 2.8$	RADAR scatterometry ('compatible' with water ice)	*Wye et al.* [2007]	
	1 of 2 'averaged' surface terrains	RADAR radiometry	*Janssen et al.* [2009]	Terrain with radiometric properties similar to icy satellites.

Table 1b. (continued)

Compound	Location Including Spectral Basis	Methods of Detection Including Author's "Confidence"[b]	Group and Year	Comments
Carbon Dioxide, CO_2	Huygens Landing Site	GCMS (tentative)	*Niemann et al.* [2005]	
	5-μm bright Tui Regio region	VIMS	*McCord et al.* [2008]	Reasonable candidate…inferred by spectral feature *near* 4.92 μm. Note the observed feature at 4.92 μm is shifted over 20 nm from the CO_2 therefore does not match. This study.
	2.74 μm abs. in surface spectra	ISO	*Coustenis et al.* [2006]	Possible but not exactly at right position nor with the correct shape.
	Disk-averaged dielectric constant $\kappa \sim 1.75 - 2.50$	RADAR reflectivity	*Zebker et al.* [2008]	Incompatible with water ice; $\kappa > 3$.
Ammonia, NH_3	Select locations in 'dark terrain'	VIMS (could contribute to slope)	This study	
	Select bright areas	VIMS (could contribute to slope)	*Nelson et al.* [2009]	
'Yellow Tholin'	Huygens Landing Site	DISR (to fit red slope in the visible)	*Tomasko et al.* [2005]	
Neutral Absorber	Huygens Landing Site	DISR (to fit blue slope from 0.83 to 1.42 μm)	*Tomasko et al.* [2005]	
'Dark Tholin' (Tholin 4 of Cruikshank, 1991)	Disk-averaged surface spectra	UKIRT and IRTF (to fit blue slope > 1.5 μm)	*Griffith et al.* [2003]	

[a]Notes: This paper comments on the findings. Slopes or albedo differences can not usually be used to determine composition.

[b]GCMS, Gas Chromatograph and Mass Spectrometer aboard Huygens probe; VIMS, Visual and Infrared Mapping Spectrometer aboard Cassini spacecraft; UKIRT, United Kingdom Infrared Telescope on Mauna Kea, Hawai'I; IRTF, Infrared Telescope Facility on Mauna Kea, Hawai'I; ISO, Infrared Space Observatory operating in Earth orbit from 1995 to 2006; ESO – ISAAC, European Southern Observatory Infrared Spectrometer and Array Camera in Chile; DISR, Descent Imager and Spectral Radiometer aboard Huygens Probe; RADAR, Radar using the communication/navigation antenna aboard Cassini spacecraft.

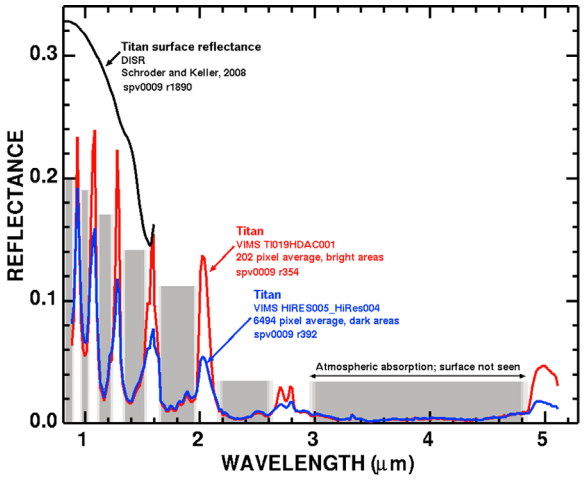

Figure 1. Representative VIMS spectra of Titan bright and dark areas. Grey bands indicate where Titan's surface is not seen in the VIMS data due to atmospheric absorption and scattering. The derived DISR spectrum [*Schroder and Keller*, 2008] is shown for comparison. Both the VIMS and DISR spectra indicate a strong blue slope to the Titan spectra.

window from 4.85 μm to the end of the VIMS spectral range, 5.1 μm (VIMS channels 336–352). Absorption and scattering in the atmosphere reduce visibility away from the peak reflectances illustrated in Figure 1. The double peak in the 2.7-μm window includes several channels. In this paper, data in the first of the double window are averaged with 3 channels: 206 to 208 at 2.681, 2.696, and 2.722 μm. The second window includes VIMS channels 212 and 213, or 2.781 to 2.798. The ratio of the I/F (observed intensity divided by the solar spectrum where πF = the solar spectrum, I and F in the same units) values for these two averaged wavelength windows is referred to as the 2.78/2.68 ratio, or simply 2.8/2.7 ratio. In this paper, regardless of which designation is used, the computation is always the same.

[7] The VIMS occultation data [*Bellucci et al.*, 2009] shows important properties concerning Titan's windows, at least as low as the occultations probe (~80 km above the surface, but over a very long path length). 1) The 5-μm window shows the highest transmission and no strong spectral features at the spectral resolution of VIMS. 2) The 2.65 to 3.1-μm window is also a high transmission window with only weak spectral features. This window shows a similar reflectance spectral structure as does Saturn's atmosphere at VIMS resolution. VIMS spectra of Titan's surface and low-lying clouds, however, show distinctly different shapes and levels than the occultation spectra (compare Figures 1, 3a, and 3b). VIMS images of the 2.8/2.7-μm ratio also show surface detail, but the low albedo and low solar intensity means only long integration time VIMS cubes show this ratio clearly (Figure 2c). When the VIMS integration time is too short, the signal is weak causing residual circles to show in the ratio (Figure 2c) due to a quantized flat field. The appearance of the flat field pattern can be used as a data quality flag: when the pattern shows, the image cubes have too low signal-to-noise ratios to detect absorption features at wavelengths longer than 2.6 μm, including in the 5-μm window.

[8] Unfortunately, the solar flux in the 5-μm wavelength region is weak and VIMS has difficulty acquiring high signal-to-noise ratio data over a large area at high spatial resolution due to limited observation time close-in during a Titan flyby. Close flyby data has mostly been acquired at 80 ms/pixel and shorter to obtain relatively high spatial resolution imaging. An exposure time of 160 ms/pixel or longer is needed for good compositional work in the 2.7 and 5-micron windows. Nevertheless, some VIMS data provide excellent information in this window and a careful search shows (below) that multiple absorption bands can be used to create maps of Titan's surface which locate the compounds responsible for the spectral features and are consistent with surface geology.

[9] It has been known since the 1990s [*Lemmon et al.*, 1993, 1995; *Griffith*, 1993; *Coustenis et al.*, 1995, *Lellouch et al.*, 2004, and references therein] that there are albedo patterns on Titan's surface. Albedo differences are not necessarily compositional variations. For example, consider a frozen lake of pure water that appears almost black compared to bright, fine-grained snow which have markedly different albedos and spectral slopes but have the same composition. Both reflectance levels and spectral slopes change with grain size; more than albedo and color variations are needed to prove variability in surface composition.

[10] Initial work by *Sotin et al.* [2005] and *McCord et al.* [2006] on VIMS data found that most of the spectral signatures were similar and could be modeled to first order by scaling the reflectance up and down with bright and dark area albedo. However, ratios of the reflectances observed through Titan's spectral windows show small variations in spectral slope, which could be displayed as a range of colors in color ratio composite images (Figure 2) [*Sotin et al.*, 2005; *McCord et al.*, 2006; *Le Mouelic et al.*, 2008, Figure 11], illustrating that variations in surface composition possibly exist across Titan, although such variations might, in theory, be due to a single compound varying in grain size.

[11] During a typical flyby of Titan, the VIMS and other optical remote sensing instruments on board the Cassini spacecraft observe Titan at a variety of solar incidence, emission and phase angles. Figure 4 illustrates the changes in VIMS spectra at varying viewing geometries. As phase angle increases, scattering contributes a greater portion of the observed signal, but the effect is minimal in the windows, and does not add to or change the basic spectral shape of the windows.

[12] Figure 5 (model 1) illustrates the principal gases in Titan's atmosphere that absorb in the VIMS spectral range (dominated by methane); the white regions denote atmospheric "windows" through which substantial solar radiation reaches the surface. The MODTRAN™ 5 radiative transfer code (developed collaboratively by Air Force Research Laboratory and Spectral Sciences, Inc.,) [see *Anderson et al.*, 2006] was used to generate this model. Shown is the two-way transmission for a vertical path through the atmosphere; no aerosols (either scattering or absorbing) were included for this simple case. In the visible wavelengths, aerosol scattering is so dominant that the surface is almost completely obscured in these atmospheric windows. At wavelengths longer than ~1μm, haze scattering rapidly falls off such that VIMS can most clearly view the surface in the 1.3, 1.6 and 2.0 μm windows. Although aerosol scattering drops off

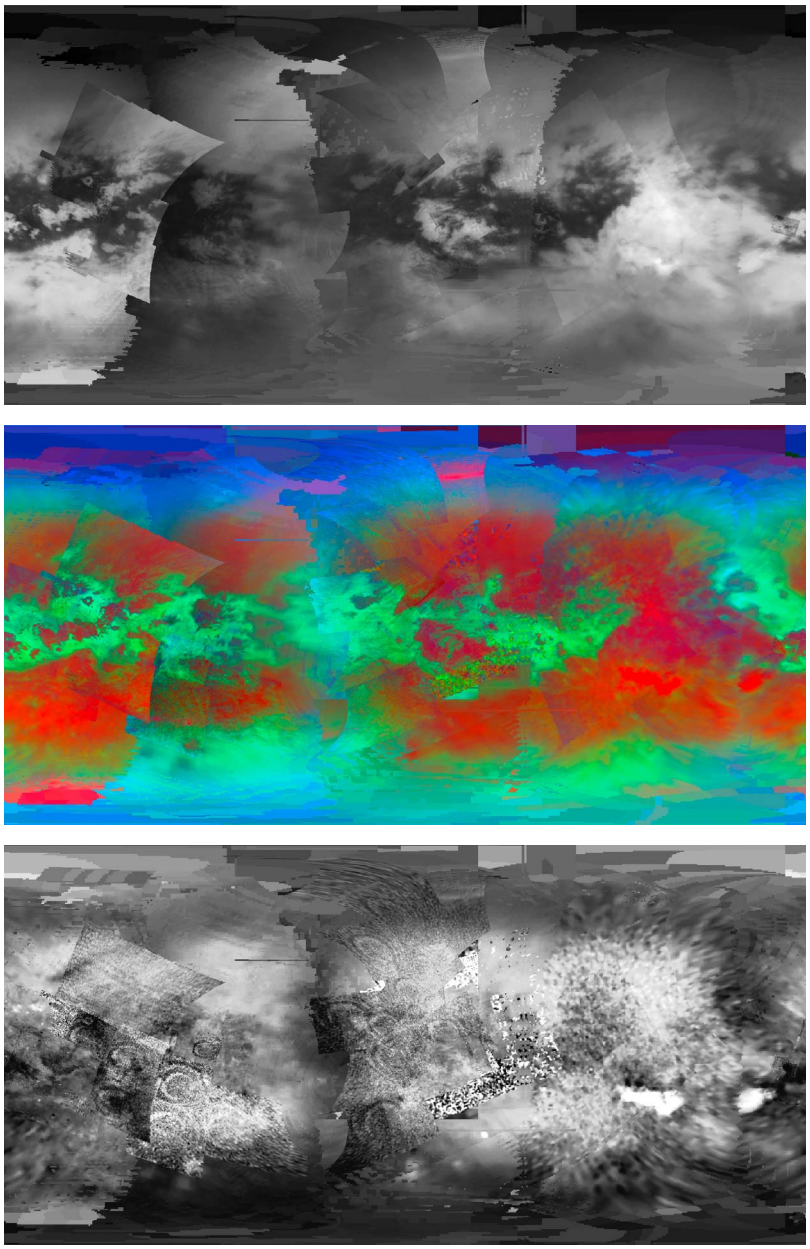

Figure 2. (a) VIMS global mosaic at 2-μm. (b) Color ratio composite: red = 5-μm reflectance, green = 2 /1.6 μm reflectance, and blue = 5 divided by 2 μm reflectance. The various colors indicate composition and/or grain size differences on Titan's surface. (c) The VIMS 2.78/2.68 μm reflectance ratio for Titan shows small differences on the surface. The rings are flat field quantization effects with short integration time image cubes. These cubes cannot be used for mapping absorption features in the 2.7 nor 5-μm windows.

much further toward longer wavelengths, the solar flux and surface reflectivity also decrease, making surface imaging again more difficult (with low signal-to-noise ratio).

[13] The model in Figure 5 (model 1) also illustrates absorption from nitrogen on the side of the 2-μm window. This window is used by some studies to derive cloud heights on Titan [e.g., *Griffith et al.*, 2005, and references therein] which did include the effects of nitrogen.

[14] For wavelengths shorter than ~1.05 μm we used the correlated-k absorption coefficients for CH_4 developed by Karkoschka of the University of Arizona [*Tomasko et al.*, 2005, and E. Karkoschka, personal communication, 2008] and for longer wavelengths we used those published by *Irwin et al.* [2006]. A broad collision-induced absorption band by N_2 centered near 4.3 μm and various absorption bands of CO were modeled with the data sets supplied inboard with the MODTRAN™ 5 radiative transfer code. Centered near 2.15 μm is a combined collisional absorption by N_2 and H_2 that was modeled with data from *McKellar* [1989] (note the 2.03-μm window is shaped by this absorption on the long wavelength side and by CH_4 on the

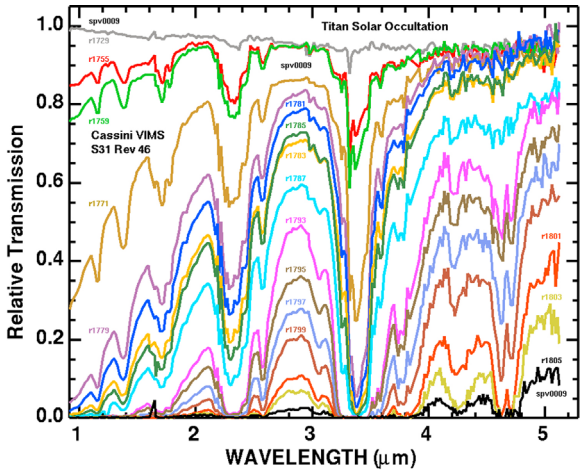

Figure 3a. VIMS solar occultation showing varying path lengths through Titan's atmosphere for Rev 46. The data indicate that the 2.7 and 5-micron windows have high transmission with no strong spectral features. The altitudes for the 15 spectra in Figure 3a are given as the bottom 15 occultation points in Figure 6d with the lowest spectrum corresponding to about 80 km altitude.

short wavelength side). Of special interest in the discussion that follows is the character of the methane windows that are expected in the 2.6 to 3.-μm region.

[15] Recent VIMS observations of solar occultations by Titan's atmosphere allow a direct comparison with the CH_4 absorption coefficients, particularly those of *Irwin et al.* [2006] that cover the 1–5-μm region: the region of greatest interest for VIMS spectroscopy of Titan's surface. The models that are shown in Figure 6a employed a 15-layer spherical shell model using the vertical pressure profile and vertical distribution of CH_4 measured by the Huygens HASI and GCMS [*Fulchignoni et al.*, 2005; *Niemann et al.*, 2005]. Also shown is a model for

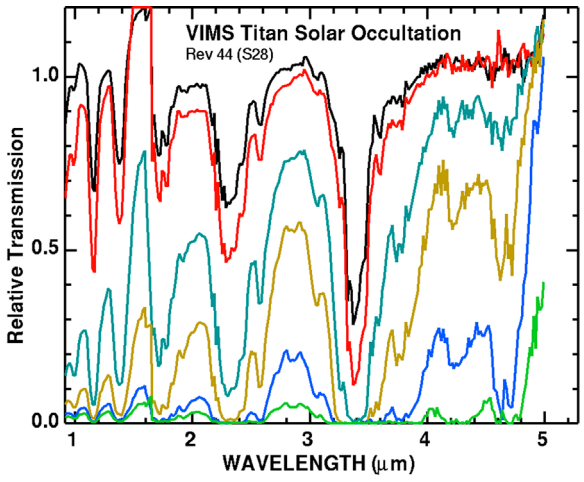

Figure 3b. VIMS solar occultation showing varying path lengths through Titan's atmosphere for Rev 44. The data indicate that the 2.7 and 5-micron windows have high transmission with no strong spectral features. The 1.6-μm window in this Rev indicates particles similar to this size caused enhanced forward scattering.

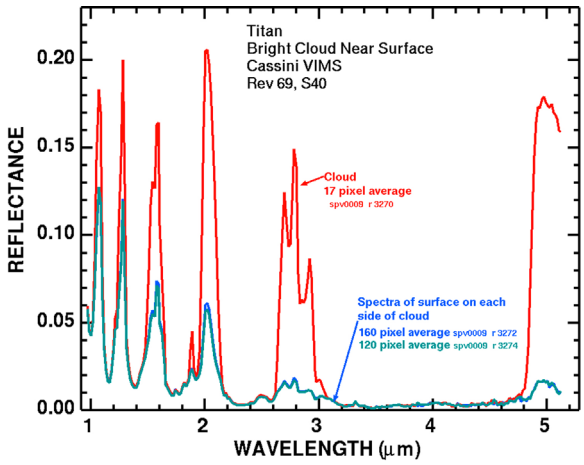

Figure 3c. Spectrum of a bright, low-lying cloud near 92°E, 18°S in Cassini Rev 69, May 28, 2008. This spectrum sets limits on the amount of absorption over the VIMS range due to the atmosphere.

the two-way transmission for a vertical path through the atmosphere (Figure 6a, bottom spectrum).

[16] We also compared VIMS data to a second atmospheric model (model 2). To compute the vertical transmission of Titan's atmosphere, we use a plane-parallel radiative transfer code that includes the main atmospheric gases absorptions and a simple haze scattering treatment [*Rodriguez et al.*, 2009]. Optical properties of the gases are pre-calculated using a high-fidelity model [*Rannou et al.*, 2010], taking into account Titan's major gaseous contributions in the near-infrared range, which are CH_4 ro-vibrational absorptions, H_2-N_2 collisions induced absorptions and Rayleigh scattering by molecules. At wavelengths longer than 1.5 μm, the methane absorption is computed with the data set published by *Boudon et al.* [2004]. At wavelengths shorter than 1.5 μm,

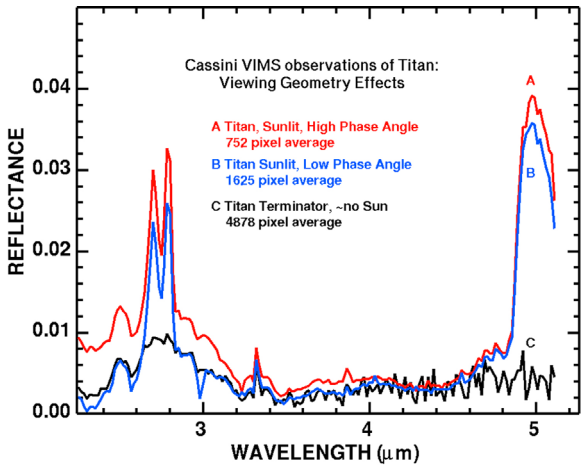

Figure 4. VIMS spectra of Titan at different viewing geometries. Low phase is an average of pixels at less than 30 degrees. High phase is around 90 degrees on well lit areas in the same general terrain as the low phase data. The terminator spectra have incidence ~90 degrees and emission near zero degrees.

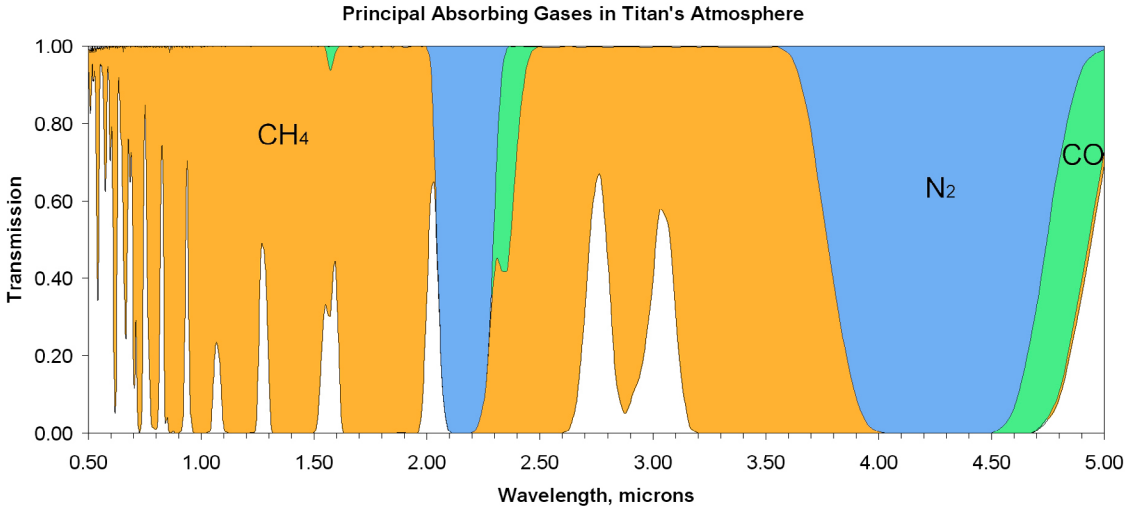

Figure 5. Dominant absorbing gases in the Titan atmosphere over the VIMS spectral region.

recent corrections for the *Irwin et al.* [2006] band model are used [*Tomasko et al.*, 2008a]. The spatial distribution of the haze is derived from in situ measurement of DISR instrument onboard the Huygens probe [*Tomasko et al.*, 2008b] and the haze layer is assumed to be made of spherical particles. In order to compute the haze optical properties, we use values of optical constants published by *Khare et al.* [1984]. This model better reproduces the complex 2.7-μm region than model 1 (Figures 6b and 6c) in both amplitude and shape. However, model 2 still shows greater absorption in the wings of the 2.7-μm window than is observed by VIMS.

[17] Model 2 gives a Titan atmospheric 2.78/2.68-μm transmission ratio of 0.97, consistent with what is observed in the solar occultation data (Figure 6d). The scattering efficiency is pretty flat within this region and does not affect the ratio much.

[18] VIMS has observed low clouds on Titan's surface. One of the lowest and brightest yet observed was on the Rev 69 Titan flyby. The spectrum of the cloud shows a scattering level and absorption on the wings of the windows close to spectra of the surface, indicating the cloud has an altitude very similar to the surface [*Griffith et al.*, 2009]. The cloud had disappeared by the next orbit. Spectra of the cloud (Figure 6c) are shown compared to the atmospheric model spectra from Figure 6a (bottom spectrum) and Figure 6b convolved to VIMS sampling and band passes. It is clear that atmospheric model 1 over-predicts absorption in the 2.8-μm window for vertical 2-way atmospheric path but appears similar to higher altitude occultation data. Atmospheric model 2 does a better job and predicts the observed amplitude correctly, and although still over-predicting absorption in the wings of the window, the spectral structure of the window appears closer to the VIMS data than model 1. The 3.1-μm window in model 1 in the model does not appear in the VIMS data, nor in model 2. Thus, while other windows appear similar to observed VIMS data, the two models do not match VIMS data for the 2.8-μm window but model 2 is closer.

[19] Because current atmospheric models are still not predicting the 2.8-μm window accurately enough, we examined solar occultation data, low clouds and surface data versus phase angle. The ratio of observed I/F at 2.8 μm to the I/F at 2.7 μm is shown in Figure 6d for VIMS occultation data, low clouds and surface data. The occultation data shows the ratio increasing slowly to about 1.1 as the occultation probes deeper into the atmosphere. The low cloud data has a ratio of about 1.2. The surface data from Figure 4 shows that a change from low to high phase angles results in a decrease in the ratio from 1.13 at low phase angles to 1.11 high phase, and further decreases to 1.01 for 90 degrees phase with grazing incidence at the terminator and normal emission. Thus, data from occultations which directly measure the transmittance of the atmosphere, to low cloud observations, to emission phase angle data all indicate the ratio is in the range from about 1.0 to 1.2. Atmospheric model 2, which most closely matches the observed intensity

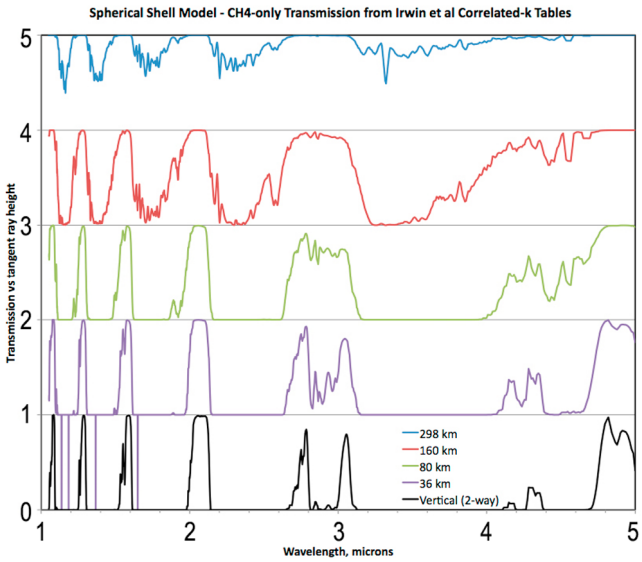

Figure 6a. Predicted solar transmission for a spherical shell model (model 1) of Titan's atmosphere including only CH_4 using correlated-k coefficients of *Irwin et al.* [2006]. Heights shown are for the tangent solar ray above the surface. For comparison the 2-way vertical transmission was computed with the same coefficients.

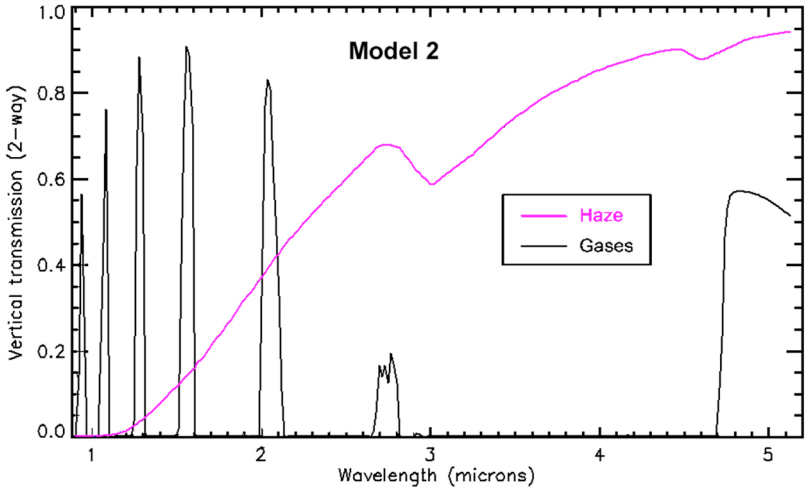

Figure 6b. Vertical transmission model (model 2) from *Rodriguez et al.* [2009].

and shape indicates the ratio is 0.97. The average of the low clouds, deep occultation points, emission-phase data, and model 2 is 1.1 +/− 0.1. If we ignore the value for model 2, the ratio raises to 1.12. This means that VIMS apparent albedo (I/F) values should be reduced by a factor of about 1.1 to get the ratio of Titan's surface reflectance. Surface spectra from VIMS data spans a larger range in the ratio than indicated by the atmospheric data, ranging from about 0.96 to 1.6 (Figure 6d). When corrected by the 1.1 factor, the ratio would range from about 0.9 to 1.5. This ratio is important because we will show below that it can be diagnostic for composition, rejecting some compounds and showing consistency with others.

3. VIMS Mosaics and Observed Titan Spectral Diversity

[20] Mosaics of VIMS data were constructed (Figure 2) [e.g., *Jaumann et al.*, 2006; *Barnes et al.*, 2007a, 2008], and were searched for the presence of spectral features using data from a spectral library and from hypothetical absorptions mathematically constructed using spectral feature shape and position mapping methods as described by *Clark et al.* [2003a]. Searches for specific mineral absorptions in the VIMS spectral range were made using data from spectral libraries [*Clark et al.*, 2003a, 2003b, 2007] recent papers on organic compounds [*Clark et al.*, 2009; J. M. Curchin et al., Reflectance spectroscopy of 2-propynenitrile, cyanoacetylene (HC_3N), submitted to *Icarus*, 2010], and using new spectra of organic ices at cryogenic temperatures measured for this study. Finally, searches for spectral features in the VIMS data were done using both mosaics and original unresampled cubes. Observed spectral diversity is shown in Figure 7.

[21] The 2.7-μm window (Figure 7a) shows variation in the 2.7/2.8-μm ratio, but no obvious spectral features. The ratio remains above 1 for most of Titan, with only small

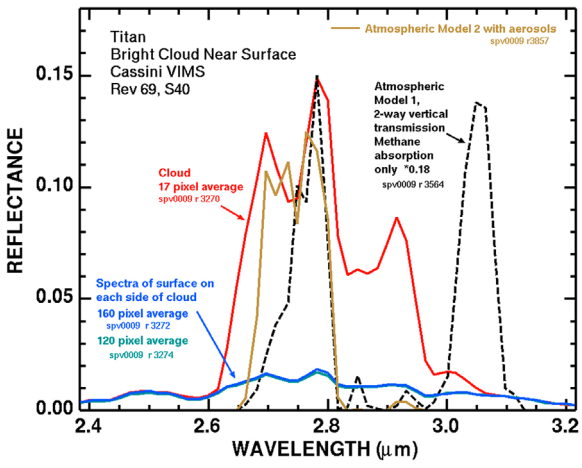

Figure 6c. Spectra of the 2.8-μm double window for the bright low-lying cloud in Figure 3c compared to the atmospheric models in Figures 6a and 6b. The model shows more absorption than actually observed in VIMS data over this window.

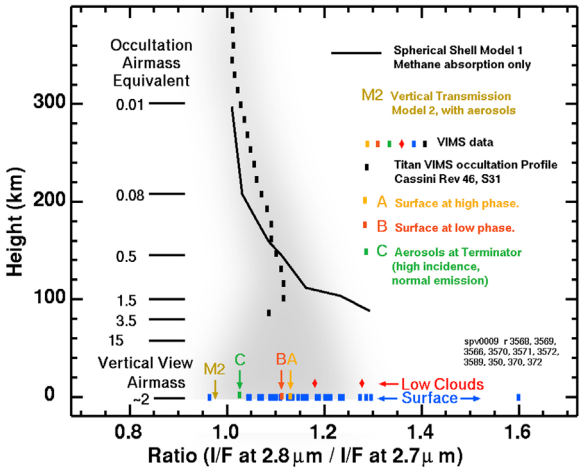

Figure 6d. The 2.8-μm/2.7-μm I/F ratio for the solar occultation data in Figures 3a and 3b, low cloud data, including that in Figure 6c, and a range of observed values of the surface viewed through the atmosphere all point to atmospheric absorption affecting the ratio by a factor of about 1.0 to 1.2. Points A, B, C are from the corresponding spectra in Figure 4. M2 is from model 2 in Figure 6b.

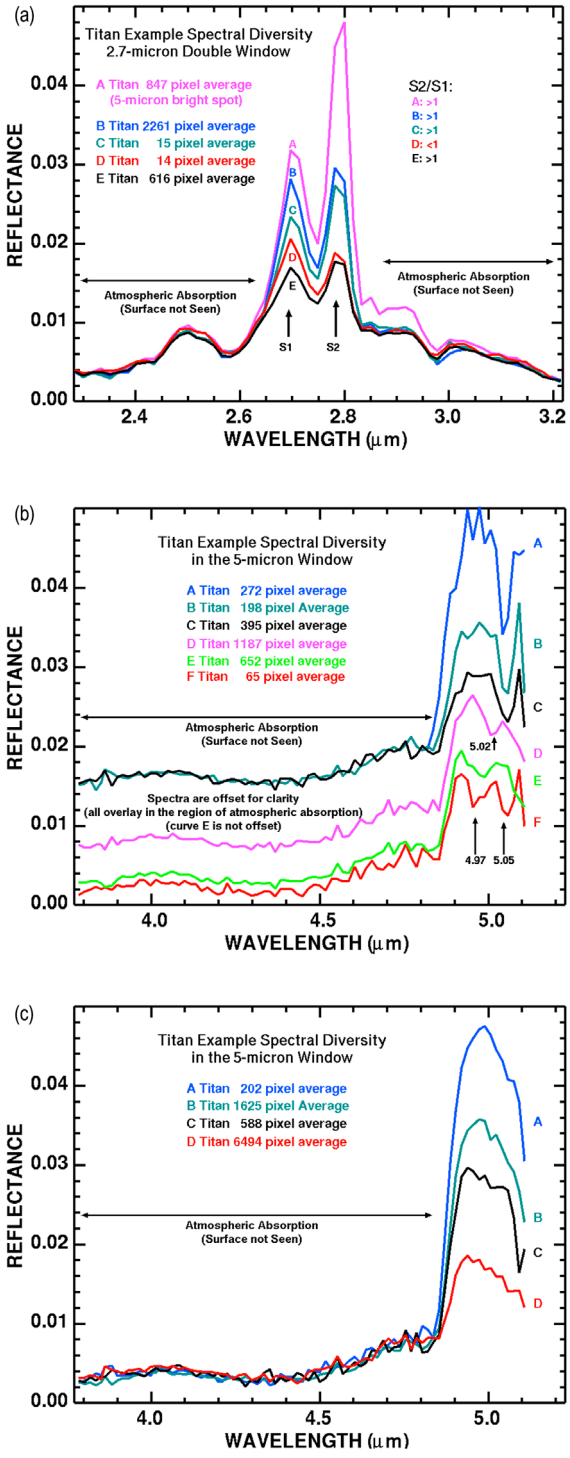

Figure 7. (a) Spectral diversity of Titan VIMS spectra. The reflectance near 2.8 μm is almost always higher than the reflectance near 2.7 μm. These wavelengths provide a strong discriminator for some compounds, including water bearing compounds and water ice, which always have the 2.8-μm reflectance lower than the 2.7-μm reflectance. The absorption between 2.7 and 2.8 μm appears to be in Titan's surface. (b) Spectral diversity of Titan VIMS spectra in the 5-μm window showing various absorption features. (c) Spectral diversity of Titan VIMS spectra in the 5-μm window showing variable shapes but no absorption features.

areas where the ratio was observed to be as low as about 0.8 in uncorrected data. Atmospheric transmission, based on the atmospheric model (previous section) and the solar occultations show that an I/F ratio in uncorrected data should be modified by about a factor of 1.1 for surface reflectance. We use a factor of 1.1 for this study, so the ratio of surface materials probably ranges from about 0.7 to 1.7.

[22] The 5-μm window shows the greatest spectral diversity. Narrow spectral features are seen within the window (Figure 7b) and on the edges of the window (Figure 7c). Absorption by surface compounds also changes the apparent shape of the window, e.g., peaked (Figure 7c, curve A) to straight sloped segments (Figure 7c, curves C and D).

[23] To date, separate spectral features at 4.91 μm ([*McCord et al.*, 2008] and shown in Figure 7b) and at 4.97, 5.01 and 5.05 μm (Figure 7b) have been found in Titan VIMS data that can be used to create maps of compositional differences on Titan's surface. An absorption feature near 5.05 μm was previously observed in atmospherically removed surface spectra (Figure 8a) [*Lellouch et al.*, 2003]. *Coustenis et al.* [2006] derived a surface spectrum for the Titan 2.7-μm window using ISO data (Figure 8b), showing a 2.74-μm absorption. The ISO data show a response similar to the VIMS

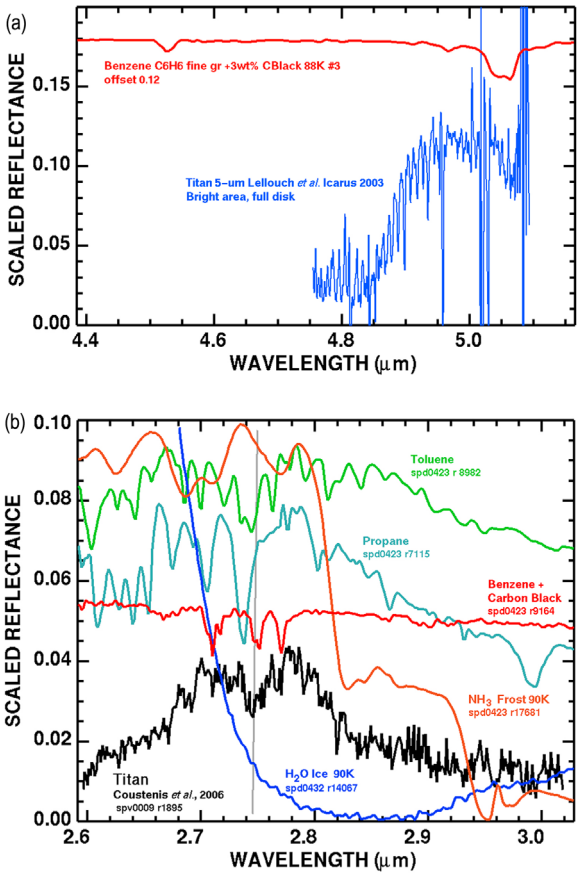

Figure 8. (a) Earth-based spectrum of Titan's surface [*Lellouch et al.*, 2003] shows an absorption near the benzene absorption position. (b) ISO spectrum of Titan's surface from *Coustenis et al.* [2006] is compared to water ice, ammonia ice, and 3 organic compounds. The ammonia and organic compounds are roughly compatible with the spectrum but the water ice is incompatible.

data (Figure 7a), but at lower spatial resolution and higher spectral resolution. The spectral features in the ISO data are inconsistent with water ice (Figure 8b) because water ice is strongly absorbing near 2.8 μm. The ice index of refraction is near unity in this spectral region, and the wing of the 3-μm OH fundamental is still strongly absorbing. All VIMS spectra of water ice-rich Saturn's satellites [e.g., *Clark et al.*, 2005, 2008, also The composition of Iapetus: Mapping results from Cassini VIMS, submitted to *Icarus*, 2010] show a minimum in reflectance near 2.85 μm, and these low reflectance levels are at odds with the Titan spectra at 2.8 μm. The 2.74-μm absorption noted by *Coustenis et al.* [2006] and seen in the VIMS spectra are consistent with only a few organic compounds measured to date. Those include benzene, toluene, and propane. Additionally, ammonia or ammonium products could contribute to the decrease in reflectance beyond the 2.8-μm peak.

4. Spectral Feature Identification

[24] We searched spectral libraries, published spectra, and conducted our own laboratory measurements of organic compounds [e.g., *Clark et al.*, 2007, 2009; Curchin et al., submitted manuscript, 2010] in order to search for matches to the spectral features illustrated in Figure 7. The VIMS 5.05-μm feature matches the position, width, and shape of a unique spectral feature due to benzene (Figure 9a, spectra T1, T2 and S4). The benzene absorption is due to an overtone of an out-of-plane bending mode whose fundamental lies near 10 μm. Pyrene has an absorption near that of benzene but is shifted to shorter wavelengths. Pyrene could contribute to the absorption and the pyrene spectrum is compatible with the Titan spectrum and the 2.8/2.7-μm ratio, which is close to 1 in both pyrene and Titan spectra, but pyrene cannot be the main cause of the 5.05-μm feature. The 5.01-μm feature is as yet unidentified, although we can rule out many compounds, including alkanes and alkenes. Aromatic hydrocarbons and nitriles have similar features that are slightly shifted (e.g., acetonitrile: Figure 9, spectrum S9, and Table 2) [see also *Clark et al.*, 2009; Curchin et al., submitted manuscript, 2010]. The 5-μm absorption in higher weight aromatic hydrocarbons shifts to longer wavelengths outside the VIMS spectral range (e.g., spectra S1, S2, and S3 in Figure 9a), leaving benzene with the unique feature identified at 5.05 μm. Higher weight aromatic hydrocarbons could possibly contribute to the downturn seen in at the end of some VIMS spectra of Titan (Figure 7c, spectra A, B, C). But of all the solid and liquid organic, nitrile, mineral and other spectra obtained here and in the literature, we find that only the spectrum of benzene matches the VIMS 5.05-μm data (Figure 9). None of the cyanide, alkyne, alkene, alkane, or other aromatic hydrocarbon spectra has a spectral feature at that wavelength. This detection of benzene by VIMS adds to the growing evidence for benzene on Titan, from the surface [*Niemann et al.*, 2005], to the atmosphere [*Coustenis et al.*, 2003] and into the thermosphere [*Waite et al.*, 2007].

[25] The 4.97-μm feature matches low molecular weight alkanes (aliphatic hydrocarbons), notably methane and ethane (Figure 9, spectra S5, S6). The observed absorption strengths indicate low optical path lengths of only a few mm represented in the spectra (discussed below). At Titan's surface temperature (~94 K) and atmospheric pressure (~1.5 bars), methane would be a liquid on the surface, and in a dry 1-bar nitrogen atmosphere of an earth-based laboratory, methane remains a liquid, even at 77 K. Ethane on Titan is near its freezing point (90 K), and dissolves nitrogen to a much lesser extent than does methane, but it is also expected to be a liquid under Titan surface conditions. The 4.97-μm feature maps predominantly in the darker areas on Titan's surface (see below), where VIMS spectra indicate that the surface would be like a wet sand with liquid methane and ethane, possibly as a slush, in which the sand could be water ice, solid organics, or a mixture. This is consistent with the detection of methane and ethane in Titan's surface by the Huygens probe at its equatorial landing site [*Niemann et al.*, 2005]. It is also possible that there is areal mixing of non-methane-ethane sites with methane-ethane pockets that are deeper but occupy a small areal fraction. The dark material forming the dune fields where liquid methane/ethane is detected might be damp or muddy at the time of the VIMS observations, but the material must have been dry at some point, to permit its transport by saltation.

[26] Propane, next in the alkane series after ethane, has a more complex spectrum but no strong feature in the 5-μm

Figure 9. Representative VIMS spectra of Titan are compared to laboratory spectra of organic ices obtained at temperatures similar to those on Titan and then convolved to VIMS spectral sampling and resolution. (a) Comparisons to aromatic hydrocarbons. Only benzene (S4) provides a spectral match to the 5.05-μm feature. (b) Comparisons to spectra of ethane (S5), methane (S6), and benzene (S4). Higher molecular weight alkanes have absorption bands shifted to shorter wavelengths. In some instances, both benzene and what appears to be methane and/or ethane map in the same locations (T3). (c) Comparison of other representative spectra to spectra of Titan. Nitriles (S9) may match the as yet unidentified 5.01-μm feature. Vertical gray bars are included to assist with comparison of band positions. The Titan spectra (T1 to T6) have strong atmospheric absorption at wavelengths less than about 4.9 μm. The lower reflectance limit in the Titan data within the atmospheric absorptions is not zero due to aerosol scattering, and the surface is not seen in the 4.4 to ~4.9-μm spectral range. Error bars are +/−1 standard deviation of the mean and include natural variations in reflectance level on Titan's surface. Laboratory spectra and the Titan spectra T3 and T5 are offset for clarity; spectra T1, T2, T4, T6, and S4 (Figure 9a) are not offset. Areal mixtures are with Carbon Black (spectrally neutral). Coarse grained refers to 100 to 300 micron diameter grains. (d) Comparison of CO_2 and HC_3N spectra at VIMS sampling and resolution between 4.5 and 5.1 μm. The HC_3N spectrum can explain the observed inflection in the VIMS data while CO_2 cannot. (e) Comparison of CO_2 and HC_3N spectra at VIMS sampling and resolution between 2.4 and 3.2 μm. The HC_3N spectrum is consistent with the VIMS data while the CO_2 spectrum is not. (f) Comparison of benzene spectra at VIMS sampling and resolution. Areas rich in benzene (based on the presence of a 5.05-μm absorption) should and do have a depression in the spectrum at 2.71 μm spectrum as seen in the red spectrum compared to the blue spectrum. The benzene "lake" is located in Figure 17b, location a.

window [*Clark et al.*, 2009] (Table 2), and only a 5% depth feature at 4.946 μm. Butane has an absorption feature at 5.06 μm, about double the width of the benzene absorption [*Clark et al.*, 2009] (Table 2). Higher weight alkanes, like decane, have a sharp 4.95-μm feature that is too short and is dissimilar in shape to the Titan absorption at 4.97 μm [*Clark et al.*, 2009]. Higher in the alkane series, paraffin also has a 4.95-μm band but it too is wider and shorter in wavelength than the Titan feature. Although many alkanes could potentially contribute to the short wavelength side of this feature, only methane and ethane could contribute to the main part of it.

[27] The 5.01-μm absorption feature in Figure 9 is not matched by any current laboratory reference spectrum, although alkynes and nitriles have similar spectral structure. Laboratory spectra of more compounds are needed to positively identify this absorption band. Acetonitrile (Figure 9c, spectrum S9) has the most similar spectral shape and position to this feature of any organic compound yet measured in reflectance, but it is not a perfect match.

[28] *McCord et al.* [2008] reported an inflection in a subset of VIMS spectra at 4.91 μm and identified the feature as carbon dioxide, although they noted that the carbon dioxide absorption is shifted in pure CO_2, so the CO_2 would have to be in another matrix to cause such a shift. The VIMS wavelengths match the positions of absorption features in water, methane, carbon monoxide, and other atmospheric lines to within 2 nm in spectra of Titan, Saturn, the rings and satellites (see numerous VIMS references in this paper and references therein). The CO_2 position required in the McCord et al. study

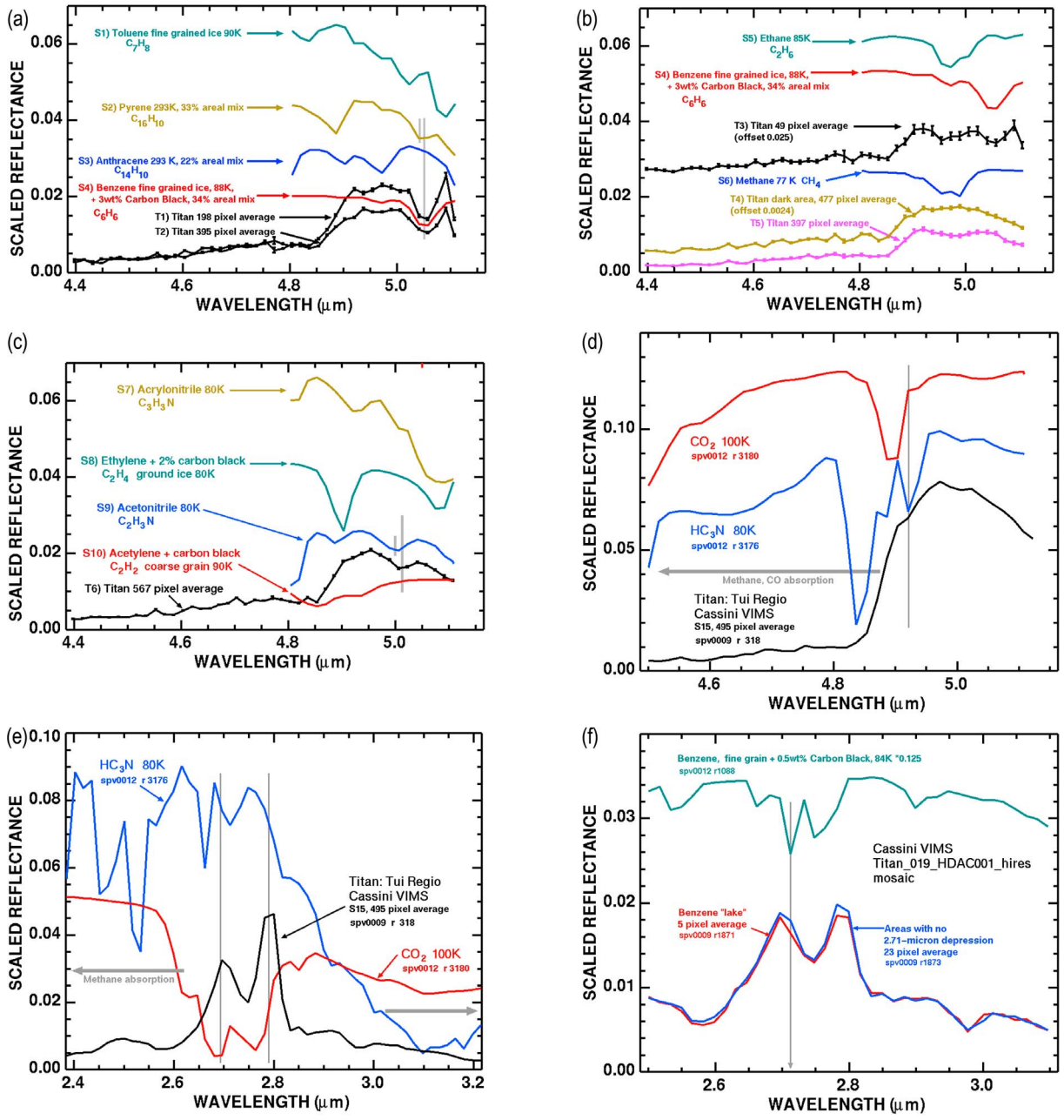

Figure 9

Table 2. Spectral Features in Titan's 5 Micron Window and the 2.6–2.8 Micron Window Are Compared

ID	Title	Center	Width	Depth	2.78/2.67 Micron Ratio
	spv0009				
512	Titan HIRES005_HiRes004 185px T1	5.053	0.042	0.407	1.205
596	Titan TI019HDAC001 288px T2	5.055	0.052	0.381	1.127
600	Titan TI019HDAC001 49px T3	4.958	0.047	0.233	1.109
		5.056	0.045	0.289	
564	Titan TI019HDAC001 477px T4	-	-	-	
604	Titan TI019HDAC001 3972px T5	4.982	0.068	0.135	1.146
580	Titan TI019HDAC001 567px T6	5.008	0.039	0.153	1.157
	spv0012				
1088	Benzene C6H6 fine grained +0.5wt% Carbon Black 84K #4	4.968	0.029	0.174	1.086
		5.050	0.050	0.774	
636	Benzene C6H6 Ice 80K #6	4.967	0.030	0.139	1.090
		5.051	0.047	0.659	
846	Benzene C6H6 Ice 80K #1	----			1.142
		5.051	0.045		
858	Benzene C6H6 Ice 80K #1	----			1.330
		5.049	0.062	.774	
648	Methane CH4 liquid, 77K #1	4.984	0.068	0.572	1.215
656	Methane Liquid 77K #13 (thin)	4.986	0.056	0.041	0.969
908	Ethane C2H6 85K #3	4.968	0.068	0.719	1.753
930	Propane C3H8 vfine 76K #2	4.869	0.016	0.051	0.776
		4.946	0.035	0.051	
		>5.1 um			
1286	Butane C4H10 frost 91K #5(doublet at 5.04, 5.07 microns)	5.06	0.07	0.56	0.995
1246	Pentane C5H12 #4 86K	4.857	0.050	0.262	1.069
		4.935	0.039	0.394	
		5.007	0.022	0.284	
1256	Hexane C6H14 #3 87K	4.939	0.074	0.474	1.028
		4.998	0.031	0.177	
1276	Heptane C7H14 #4 92K	4.944	0.062	0.439	1.028
		5.038	0.031	0.248	
1264	Octane C8C18 #3 87K	4.871	0.025	0.244	1.075
		4.948	0.051	0.373	
		5.006	0.018	0.218	
		5.066	0.032	0.200	
1398	Nonane C9H20 #3 85K	4.942	0.077	0.377	
		5.006	0.017	0.103	
		5.061	0.030	0.208	
516	Decane C10H22 ice 125K #3	4.951	0.057	0.353	0.842
		5.037	0.036	0.173	
		>5.1 um			
402	K-Fe-CN 0.95 + 0.05 CLB	4.922	0.022	0.079	0.806
416	Pyrene C16H10 CAS 129-00-0	4.883	0.051	0.365	1.039
		4.977	0.034	0.100	
514	paraffin C22-25H46-52gfwax 273K	4.950	0.084	0.521	1.122
		>5.1 um			
524	acrylonitrile C3H3N 80K #2	4.922	0.050	0.180	0.792
		5.09	>0.1	~0.8	
568	HCN + H2O ice D 76K	4.840	0.030	0.039	0.634
		5.023	0.017	0.022	
694	Acetonitrile C3H3N Ice 80K #5	4.888	0.030	0.130	1.314
		4.999	0.048	0.179	
		>5.1 um			
900	Naphthalene C10H8 #3	4.917	0.044	0.304	0.922
		5.026	0.042	0.190	
		>5.1 um			
1000	Acetylene C2H2 coarse grain + Carbon black 3 90K #4	4.854	0.139	0.262	0.951
	(absorbs short wavelength half of Titan window)	S 4.936	0.036	0.051	
1006	Ethylene C2H4 frost 92K #3	4.900	0.040	0.492	0.925
		5.077	0.045	0.226	
1054	Propyne C3H4 84K #2	4.849	0.043	0.448	0.828
1056	Carbonyl Sulfide frost 120K	5.04	0.2	0.6	1.159
	(absorbs short wavelength	asymmetric			
	2/3 of Titan window)				
1068	Anthracene C14H10 293K	4.899	0.028	0.083	1.143
		4.970	0.043	0.179	
		>5.1 um			
1070	Pyrene C16H10 293K	4.885	0.037	0.169	1.020
		5.042	0.032	0.098	
		>5.1 um			
1080	Toluene C7H8 fine grained 90K #5	5.021	0.033	0.206	1.061

Table 2. (continued)

ID	Title	Center	Width	Depth	2.78/2.67 Micron Ratio
		5.083	0.032	0.407	
1118	Tholin Run80EET N2:CH4:CO2 = 90:5:5	none		<0.003	0.227
1164	Naphthalene crse grnd 105K #8	4.906	0.042	0.394	0.985
		4.985	0.027	0.123	
		5.025	0.021	0.350	
		>5.1 um			
1188	Xylenes C6H4(CH3)2 86k #4	4.930	0.038	0.099	1.114
		4.997	0.035	0.087	
		>5.1 um			
1198	Cyanonaphthalene 84K #5	4.928	0.032	0.133	0.829
		5.066	0.059	0.719	
734	H2O ice fine ground 86 K	----			0.048
774	H2O ice fine grained + 0.2 wt% carbon black 90K	----			0.130
712	block H2O ice Flash Frozen 80K	----			0.353

would need to be shifted over 20 nm to match the 4.91- μm position observed in the VIMS spectra (Figure 9d). We can find no study that reports such a large shift of this absorption feature of CO_2 under any conditions. Second, the spectrum of CO_2 in the 2.7-μm region is not consistent with the observed spectrum of Titan. Therefore, we find this scenario implausible and find another compound, a known Titan atmospheric component, cyanoacetylene, or HC_3N (Figures 9d and 9e) better matches all spectral windows. HC_3N has an absorption at 4.91 μm (Curchin et al., submitted manuscript, 2010) which at VIMS resolution and sampling produces the correct response at 4.91 μm (Figure 9d). Spectra of HC_3N are also compatible with the 2.7–2.8- μm window (Curchin et al., submitted manuscript, 2010) whereas CO_2 is not because it strongly absorbs most of the window (Figure 9e). HC_3N is a predicted photochemical product of methane and nitrogen in Titan's atmosphere [*Yung and DeMore*, 1999, and references therein]. We stress, however, that the VIMS spectral resolution is not high enough to positively identify HC_3N, just that it is a better fit than CO_2 to the Titan spectrum and that CO_2 can be ruled out as the origin of the 4.91-μm spectral feature because it is too shifted to match the observed spectral structure.

[29] Detection of HC_3N in the solid state in Titan's atmosphere is tentative, and is based on the observation of a 505 cm^{-1} (19.8 μm) shoulder in a few of the Voyager Infrared Imaging Spectrometer (IRIS) spectra of Titan's stratosphere [*Samuelson*, 1985, 1992]. Further Earth-based work with the Infrared Space Observatory (ISO) has made the case stronger, but still not definitive [*Hudson and Khanna*, 1987; *Coustenis et al.*, 1999, 2003]. Additional work on the 505 cm^{-1} absorption feature in the laboratory at temperatures from 15 to 150 K led *Khanna* [2005] to conclude from the Voyager IRIS data that crystalline cyanoacetylene is indeed present in Titan's stratosphere, along with evidence for solid acetylene. More recently, analysis of thermal emission in the far infrared observed with the CIRS aboard Cassini has found compelling spectral evidence for the crystalline ν6 HC3N feature at 505 cm^{-1} [*Anderson et al.*, 2010].

[30] The spectrum of benzene is also compatible with Titan's 2.7-μm window (Figure 9f). Benzene has a 2.71-μm absorption, which at VIMS resolution, should show as an indicator in VIMS spectra. The 2.71-μm absorption is only one VIMS channel wide, but areas containing the 5.05-μm absorption show consistency at 2.7 μm. The inflection at 2.71 μm maps in the same areas as does the 5.05-μm absorption, as discussed in the section on mapping below.

[31] Laboratory spectra of hydrocarbon compounds within a series like the alkanes show similar spectral properties, but other series show different spectral properties [*Clark et al.*, 2009]. For instance, compare the spectra of the alkanes, methane and ethane, to the aromatics, benzene and toluene, in Figures 9 and 10. Even in the narrow spectral range of Titan's 5-μm window, there are enough unique absorption features and feature positions in most spectra of organics to allow one to distinguish between the two classes on Titan's surface at VIMS spectral sampling and resolution. Higher spectral resolution covering the full Titan 5-μm window, ~4.8 to 5.6 μm, could show a wealth of spectral detail, and representative spectra are shown in Figure 10.

[32] The spectral response of compounds within Titan's methane windows was also analyzed. We computed the reflectance and reflectance ratios for lab spectra of organic, ammonium, nitriles, OH and water bearing compounds, as well as for certain minerals at VIMS sampling and resolution. We found that the 2.8/2.0-μm reflectance ratio and the 2.8/2.7-μm reflectance ratio provide good discrimination among classes of compounds (Figure 11). The 2.8/2.7-μm reflectance ratio is low (less than about 0.3) for water ice and compounds containing water. As the water content

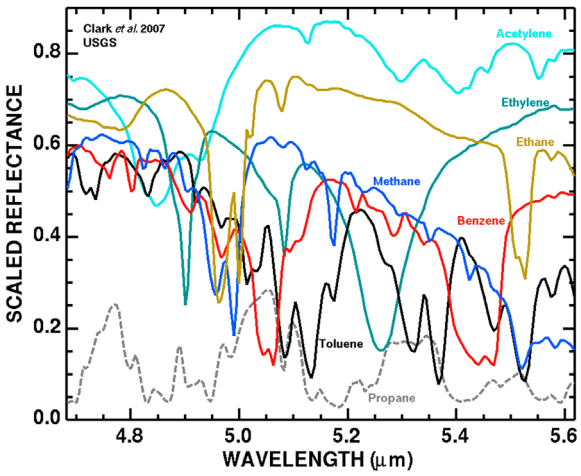

Figure 10. Higher spectral resolution data and broader spectral coverage than VIMS provides through the Titan 5-μm window could show spectral features like those shown here for 7 organic compounds. The spectral resolution ($\lambda/\Delta\lambda$) is 500 (sampling = 2 wave numbers).

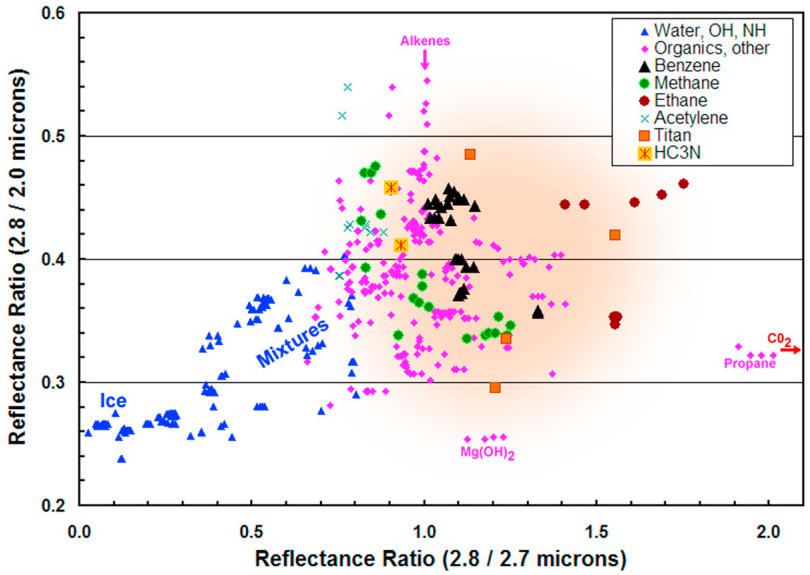

Figure 11. Band ratios in Titan windows indicate compatibility with classes of compounds. Laboratory data (points) were convolved to VIMS spectral resolution and sampling, then the same spectral channels were averaged to produce the ratios as done with VIMS Titan spectra. Titan surface derived data (orange squares) are from [*McCord et al.* 2006], and the light orange cloud represents the observed range of ratios observed in all of Titan VIMS spectra. Using the 1.1× correction derived in this paper, the light orange cloud should be shifted about 0.1 units to the left, which better covers the cloud of organic points. The lab data does not shift, only the Titan data uncorrected for atmospheric effects should be shifted. CO_2 falls off the right edge of the plot. The ratios show that the Titan surface reflectance is compatible with a number of organic compounds but is compatible with neither water ice nor ammonium-bearing compounds. See data in Table 2.

decreases, the ratio moves closer to 1 or to the value of the reflectance ratio of the non-water bearing compound. Ammonium-bearing compounds show similar trends with ratios well below 1. Even small amounts of water or ammonia produce ratios significantly less than 1. The 2.8/2.0-μm reflectance ratio is an indicator of blue slope, and mimics other ratios indicating blue slope from 1 to 3 μm. A blue slope has been commonly invoked as evidence for water ice on Titan, but as the data in Figure 11 shows, all the compounds studied here have blue slopes. While water ice has steeper blue slopes than other compounds, larger grain sizes of many other compounds can produce slopes similar to finer grained size water ice. It is plausible that these other compounds might have a coarser grain size than that of water ice in view of the existence of vast equatorial belts of dunes that contain sand-sized particles and the dunes have a dielectric constant consistent with solid organics [*Lorenz et al.*, 2006]. All compounds containing fundamental absorptions in the 3-μm region so far studied show blue slopes in reflectance, and the blue slope increases with increasing grain size [see, e.g., *Clark et al.*, 2007, 2009; Curchin et al., submitted manuscript, 2010]. The data in Figure 11 show that organic compounds are consistent with Titan's reflectance spectrum while water and ammonium containing compounds are not. CO_2 frost is also incompatible with Titan's spectrum, plotting off the left edge. Acetylene plots slightly low compared to Titan spectra, consistent with the lack of spectral feature evidence. Benzene, cyanoacetylene, toluene, methane and ethane are all compatible. Of course, compounds such as CO_2 could be present at low enough abundances such that the reflectance ratios are not affected, meaning they are not spectrally dominant. A study would need to be conducted in order to determine what those abundances would be.

5. Liquid Methane and Liquid Ethane Depths on Titan

[33] We derived the absorption coefficients for liquid methane and liquid ethane in a 1-bar nitrogen atmosphere at about 90K (Figure 12). The laboratory setup is described by *Clark et al.* [2009]. Ethane and methane were condensed in

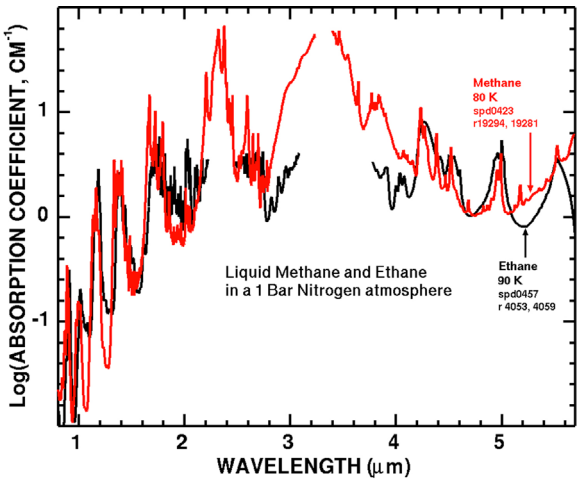

Figure 12. Derived liquid methane and liquid ethane absorption coefficients from laboratory measurements in a 1 bar nitrogen atmosphere at 80 and 90 K.

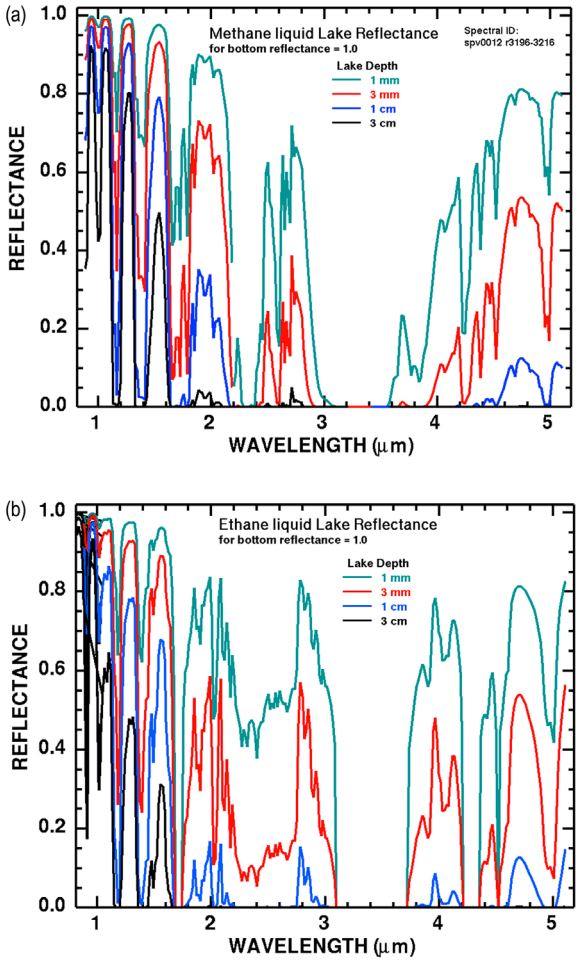

Figure 13. Computed lake reflectance assuming a bottom reflectance of 100% for 4 liquid depths of (a) methane and (b) ethane using the absorption coefficients from Figure 12.

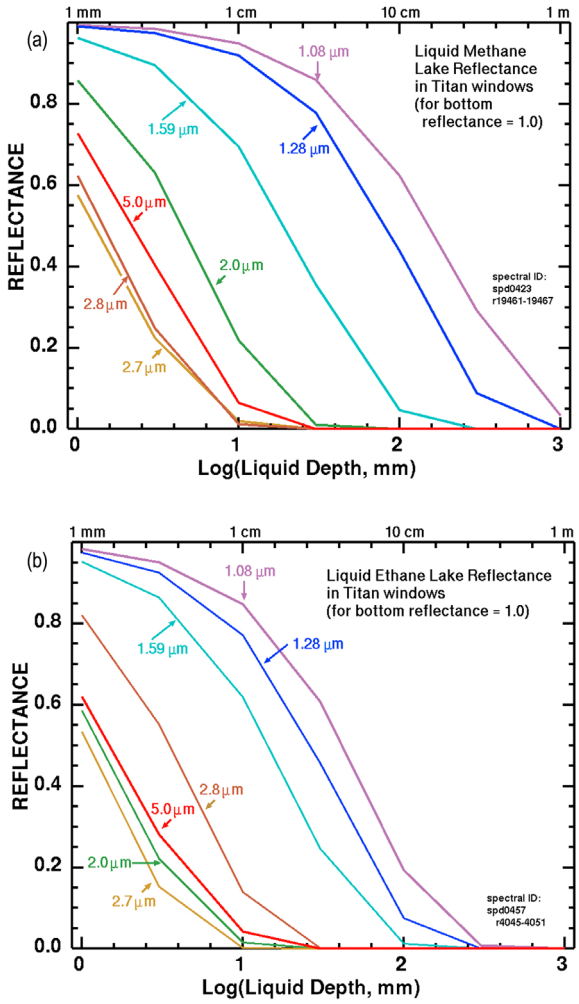

Figure 14. Reflectance as a function of lake depth for (a) liquid methane and (b) liquid ethane for Titan windows at VIMS spectral resolution and sampling.

an aluminum sample cup and a 2-way transmission spectrum was measured. The viewing geometry avoided specular reflection from the liquid surface. Path lengths for methane were 12 mm (6 mm depth), 10 mm, and 0.42 mm. The path length is accurate to about 10% and the 0.42 mm path length was determined from extrapolating absorption features in the 10 mm path to features in the 0.42-mm path spectrum. The different path lengths allowed a wide range of absorption coefficients to be measured, except in the strongest portion of the C–H stretch fundamental at 3.4 μm. The ethane was measured at one path length: 14.4 mm so only the weakest absorption features are well characterized. However, for our Titan study, only the weakest absorptions appearing in the Titan windows are of interest, so these data cover the range needed.

[34] Spectra of lake transmission (assuming a lake bottom reflectance of 100%) were computed and are presented for methane in Figure 13a and ethane in Figure 13b. Reflectances in the Titan windows for the spectra in Figures 13a and 13b are shown in Figures 14a and 14b, and the band depths for the 2 and 5-μm absorptions in liquid methane and ethane are shown in Figure 15. The data can be used to determine or at least set upper limits to the amount of liquid detectable in the optical surface using near-infrared wavelengths. Unfortu-

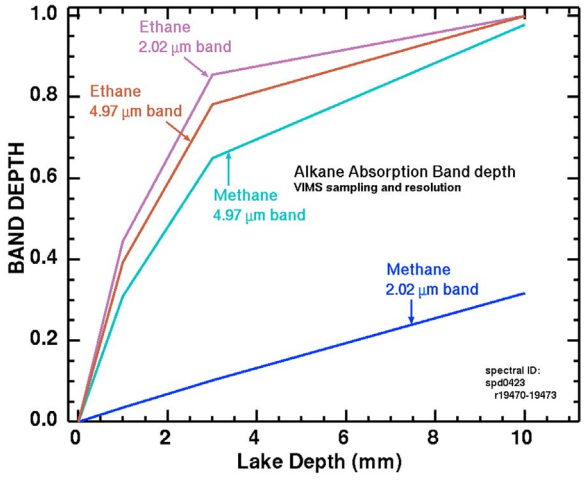

Figure 15. Absorption band depths for liquid depths over a reflecting layer for liquid methane and ethane at VIMS resolution and sampling. VIMS is sensitive to very small amounts of liquid on Titan's surface.

Table 3. Path Lengths in Cloudy and Muddy Mixtures[a]

Amount of Montmorillonite in Sample (Kg/Liter)	Path Length in H_2O – Montmorillonite (SWy-2) Mixtures				Reflectance		Observations
	0.98 μm (cm)	1.19 μm (cm)	1.34 μm (cm)	1.68 μm (cm)	1.683 μm	2.0 μm	
0.00050	10.9	5.26	2.15	1.49	0.0053	0.0052	light cloudy
0.00167	8.07	4.62	1.98	1.38	0.0048	0.0046	
0.00501	5.44	3.61	1.71	1.15	0.0013	0.0006	
0.0165	2.63	1.93	1.24	0.88	0.0051	0.0019	cloudy; plastic stick falls over
0.050	1.42	1.04	1.07	0.75	0.0179	0.0018	muddy; plastic stick stands in sample
0.100	0.70	0.60	0.50	0.43	0.0406	0.0018	muddy; can form structures several cm in size
0.300	0.41	0.29	0.26	0.24	0.1080	0.0019	thick pasty mud, difficult to make into structures due to hardness
H_2O Absorption Coefficient	0.484 cm^{-1}	1.296 cm^{-1}	3.03 cm^{-1}	5.51 cm^{-1}			

	Comparison Absorption Coefficients			
	2-μm Peaks	2-μm Continuum	5-μm Peaks	5-μm Continuum
Methane	1.90 cm^{-1} (2.0117μm)	0.54 to 0.73 cm^{-1}	2.83 cm^{-1} (4.956 μm) to 4.04 cm^{-1} (4.990 μm)	1.18 to 1.07 cm^{-1} (spd0423 r19262 W25)
Ethane	5.54 cm^{-1} (2.0298 μm)	0.75 to 0.80 cm^{-1}	4.12 cm^{-1} (4.961 μm) to 5.45 cm^{-1} (4.999 μm)	1.29 to 0.82 cm^{-1} (spd0457 r 2246 W25)

[a]Reflectance measured with incidence = 25 degrees, emission ~30 degrees, azimuth ~90 degrees, phase angle ~25 degrees. Montmorillonite wet reflectance, continuum: 0.348 at 0.95 μm, 0.406 at 1.683 μm. Reflectance at 2 μm represents specular reflection.

nately, as with all remote sensing, the VIMS data cannot probe below the near-infrared optical surface, so nothing can be concluded about conditions below that level.

[35] We consider only detectable methane and ethane. The continuum absorption in the windows and the 2 and 5-μm absorption features provide strong leverage for detecting liquid methane and ethane on Titan with VIMS. Most of Titan shows low but measurable reflectance in all of the Titan windows (Figures 1–12). Except in rare locations [e.g., *Brown et al.*, 2008] no liquid methane or ethane is detected via a 4.97-μm feature nor is any indicated by continuum absorption in Titan's windows. Brown et al. found about a 0.3 mm ethane path length in the southern lake, Ontario Lacus. The maximum path lengths found for the features in Figure 9 are about 1 mm, or liquid depths of 0.5 mm if all the liquid were above the surface and none mixed in the regolith.

[36] What might such path lengths mean for the observable surface? We conducted a study of path lengths in water using absorption at 0.98, 1.19, 1.34, and 1.68 μm as a proxy for absorptions in methane and ethane. The methane and ethane 2 and 5-μm absorption coefficients range from approximately 0.5 cm^{-1} in the continuum to about 5.5 cm^{-1} for narrow absorptions (Figure 12), compared to the water absorption coefficients of 0.48 cm^{-1} at 0.98 μm to 5.5 cm^{-1} at 1.68 μm. Thus the water absorption coefficients cover the range of methane and ethane absorption that we might observe on Titan through Titan's windows. Note that the VIMS spectral band pass of about 17nm does not resolve the sharp absorptions in methane and ethane at 2 and 5 μm, so the effective maximum absorption coefficients are approximately 3 and not 5.5 cm^{-1} in VIMS resolution data.

[37] Spectra of montmorillonite-water mixtures from *Clark et al.* [2007] and additional mixtures in that series were constructed and measured up to 0.3 kg/liter. The equivalent path length was derived and the results presented in Table 3. The montmorillonite clay is a proxy for < 2 μm particles that may be raining down through Titan's atmosphere into any liquids on the surface. As seen from Table 3, cloudy liquids have path lengths of several centimeters whereas muddy surfaces have path lengths of about a centimeter and less.

[38] The path lengths in VIMS data for Titan indicates that if the liquid were mixed in a regolith surface, the surface would be categorized as a "mud" [*Bates and Jackson*, 1976]: "a slimy and sticky mixture of finely divided particles of solid or earthy material with a consistency varying from that of a semifluid to that of a soft plastic sediment." Such path lengths would indicate a "muddy" layer in the optical surface (top few mm) rather than deep clear lakes. As noted above, the VIMS detection only includes the near-IR optical layer so the total depth of liquid is not determined. We have found no VIMS data that indicate larger path lengths indicative of deep, clear lakes of liquid methane or ethane. Note the northern lakes have yet to be imaged with enough signal-to-noise ratio by VIMS to derive composition. The first opportunity to acquire high resolution VIMS images on a northern lake will be during the T69 flyby on June 5, 2010.

[39] We also consider sub-pixel lakes. Deeper liquids that are sub pixel may contribute to the observed absorptions. However, once clear lake depths approach 3 cm, or liquid path lengths approach 6 cm (cloudy mixtures), essentially all light in the 2, 2.7 and 5-μm windows would be absorbed and no signal would contribute to observed liquid methane or ethane band depths (Figures 13a, 13b, 14a, 14b). Liquid path lengths in the 6 cm range would change the reflectance ratios in Titan's shorter wavelength windows, including the 1.3 and 1.6-μm windows. We see no evidence for significant changes in this ratio that might indicate such liquid path lengths. Liquid path lengths greater than about 20 cm would

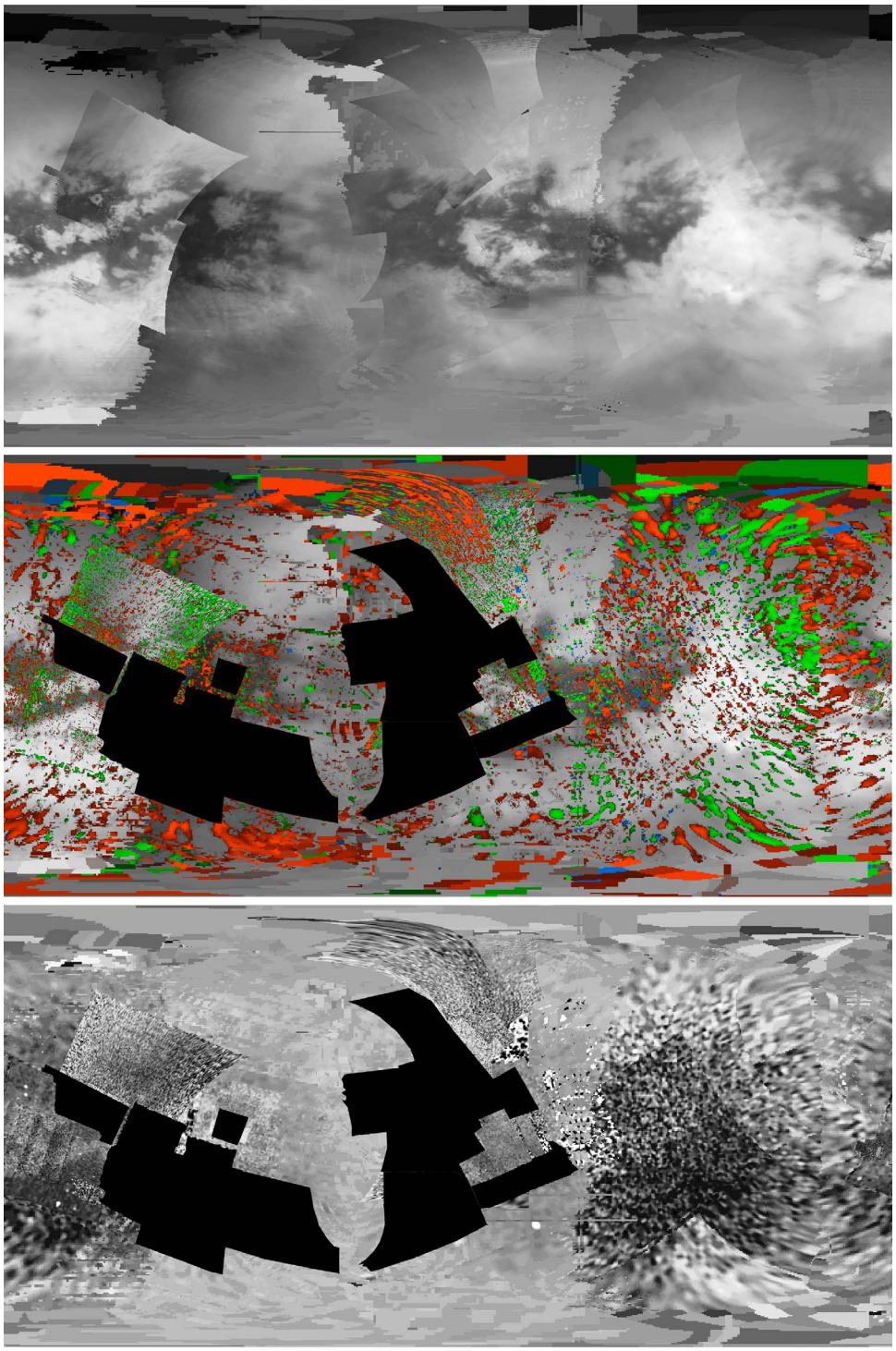

Figure 16. (top) Titan VIMS global mosaic viewed in the 2-μm window. (middle) Materials map for the 5.05-μm absorption (red), 5.01-μm absorption (green), and 4.97-μm absorption (blue). (bottom) The 2.71-μm absorption band depth.

absorb most light in the 1.08-μm and longer windows. Subpixel lakes with path lengths greater than about 20 cm would simply lower the reflectance level without contributing detectable liquid spectral signatures, thus such subpixel lakes are not detectable by VIMS.

[40] *Brown et al.* [2008] argued that the near zero I/F (~0.002 at 1 air mass) observed within Ontario Lacus and I/F ~0.01 in the areas surrounding Ontario Lacus must mean that "the lake can only have zero reflectivity if its surface is smooth and free of scattering centers greater than about 5 μm in size, the surface is viewed in non-specular geometry, and there are no slopes or facets allowing partial specular reflection along the line of sight." This led to the argument that it is unlikely that any solid surface would have such

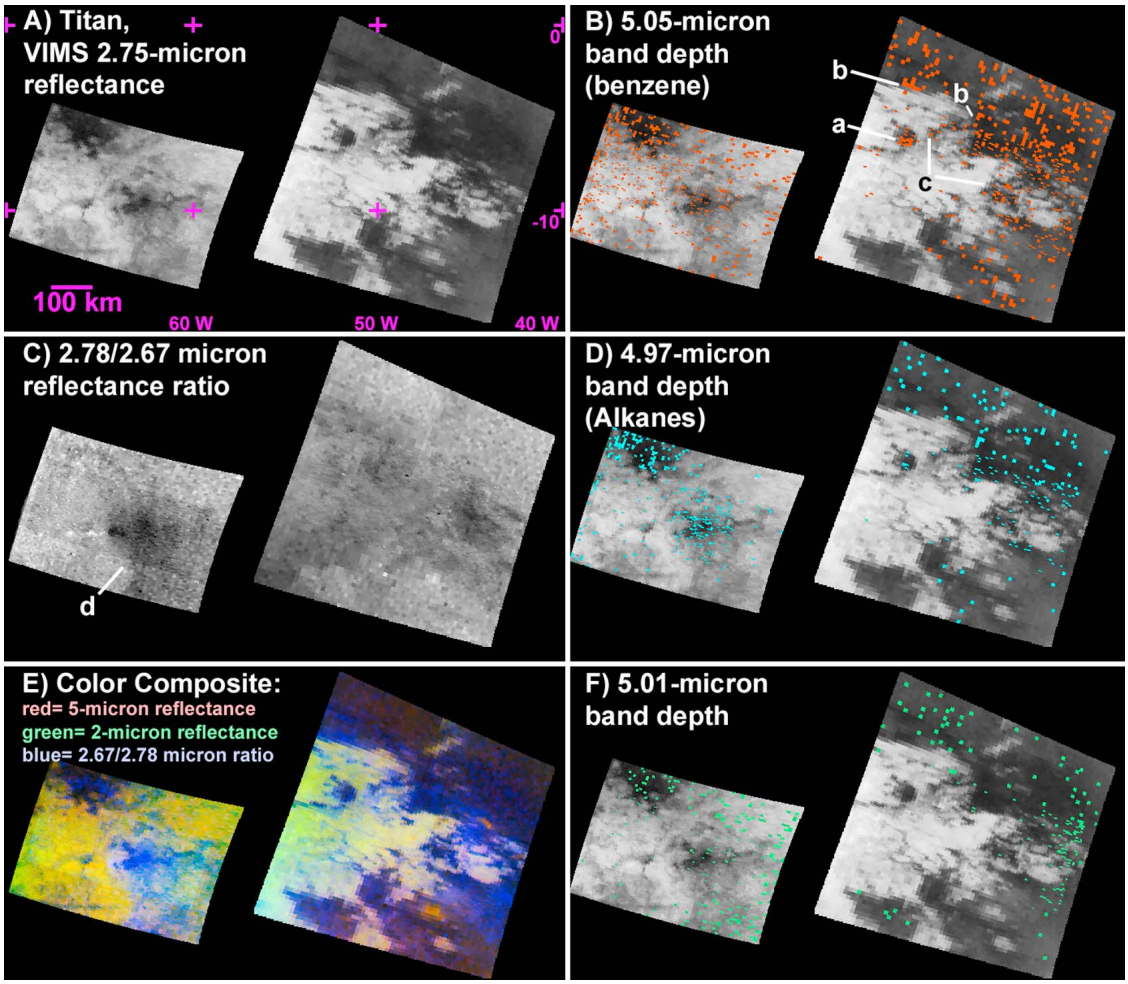

Figure 17. The highest VIMS spatial resolution mapping of Titan's surface, with adequate signal-to-noise ratios to show the distribution of the materials causing the observed absorption bands. North is up and the mosaic sampling is 2 km/pixel centered near longitude 58°W, latitude 8°S. (a) Base map at 2 μm. The spatial resolution changes because different image cubes were obtained at varying distances from Titan. (b) Benzene predominantly occurs in dark areas, bright/dark boundaries (labeled "b"), in channels (labeled "c") and, and notably, in the small circular feature (labeled "a") that appears to be a lake or basin. (c) The 2.78/2.68-μm reflectance ratio shows that a material has been diffusely painted (labeled "d") on the surface over hundreds of km. (d) Locations mapped with the 4.97-μm feature that may indicate the presence of methane and/or ethane in the surface. (e) A color composite shows structural and compositional details, notably many sinuous channels. (f) Locations of the 5.01-μm absorption.

constraints, indicating that "Ontario Lacus is filled with a quiescent liquid, free of particles larger than a few micrometers." At a latitude of 78°S, an I/F value of Ontario Lacus of ~0.002 would mean a normal reflectance of ~0.01. Further, the reflectance decrease from outside the lake to inside the lake is approximately fivefold.

[41] Our measurements of water montmorillonite mixtures show similar trends (Table 3). At the viewing geometries, with phase angles roughly comparable to the VIMS Ontario Lacus observation, but with higher incidence angle (and probably greater influence from specular reflections), the specular reflections of the cloudy mixtures is about 0.005 and decreases to about 0.002 for muddy mixtures. At the highest montmorillonite concentration, the reflectance depression is close to 4× where the absorption coefficient is ~5 cm^{-1}, similar to the results on Ontario Lacus. So the spectral properties of muddy surfaces are consistent with the small optical path lengths, the reflectance depression of the particulate-liquid mixture and the specular components observed in VIMS data on Titan. The *Brown et al.* [2008] specular reflection argument of a liquid surface is still consistent with cloudy mixtures, but the indicated path lengths and reflectance depression is not consistent with low particulate concentration (cloudy) mixtures. Thus we conclude that Ontario Lacus and the other areas where liquid methane/ethane are described in this paper are observed are consistent with a wet or muddy surface at the time of data acquisition.

[42] Could small amounts of ethane be detectable in a deep methane lake explaining the Ontario Lacus spectrum? At 2.0298 μm, the ethane absorption coefficient is 5.54 cm^{-1} (Table 3) and at that same wavelength, the methane absorption coefficient is 1.0 cm^{-1}. Thus at concentrations below about 20% in methane, ethane becomes increasingly difficult to detect, especially with a low spectral resolution instruments

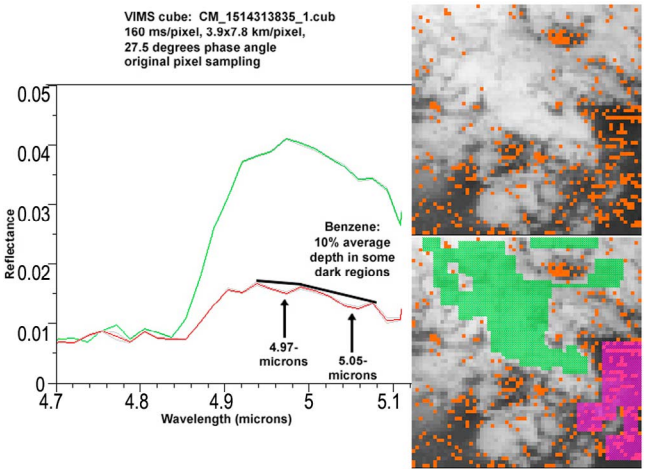

Figure 18. Block averages of bright and dark region spectra show that absorption features are consistently observed in the dark material. Red points are the 5.05-μm spectral feature-fitting results that show the strongest absorptions.

like VIMS. In a clear lake there would be competition between total absorption in both the 2 and 5-μm windows and the ability to detect a weaker ethane absorption at 2-μm. Again, if the lake depth was more than about 3 cm deep (6 cm path length), essentially all light in the 2, 2.7, and 5-μm windows would be absorbed and no ethane or methane could be detected in those windows (Figures 13–15). Similarly, we conclude that if the signals observed by VIMS were coming from the surface with the path lengths less than a millimeter, a clear lake depth of less than half a millimeter on a perfectly flat surface or a muddy surface is consistent with the observations.

[43] The VIMS-measured I/Fs for pixels within Ontario Lacus are indistinguishable from zero at 5μm. However, they are nonzero at shorter wavelengths. The flux in the centers of the shorter-wavelength windows like 2 μm could be being filled in by specular reflections from the lake surface of scattered light from the sky, as suggested by *Barnes et al.* [2009]. The wavelength dependence of the detected lake I/F, brighter in the shorter wavelength windows, supports this idea. While this scenario could account for the signal coming from the lake at the core of the ethane absorption feature, it does not however help in explaining the feature itself. Such specular sky-light cannot provide the continuum reflection that would be necessary in order to generate an absorption band in the first place. Hence although specular sky reflection modifies the reflective spectrum of Ontario Lacus in detail, it does not affect the overall conclusion for the observed liquid ethane path length. Combined with complications of the variations of diffusely scattered light as a function of wavelength, we can only conclude that the liquid depth of Ontario Lacus may only be a lower limit, as argued by *Brown et al.* [2008]. Data obtained during the T51 flyby (March, 2009) at a more favorable viewing geometry show the ethane band to be nearly 3 times deeper, supporting this view.

6. Compositional Mapping

[44] Using the spectral feature fitting methods of *Clark et al.* [2003a], the spectral features at 4.97, 5.01 and 5.05 μm were mapped using the global mosaic (Figures 2 and 16), and using selected high spectral resolution and long exposure time cubes (Figures 17, 18, 19, 20). Higher spatial resolution may be able to resolve smaller outcrops of different compounds, as is indicated in the various compositional maps: as spatial resolution increases, more pixels show absorption bands. Dark regions show greater spectral diversity in the 5-μm window as illustrated in Figures 7b and 7c, whereas bright regions tend to have higher albedo and a convex shape with little to no absorption features, as illustrated in Figures 7c (curves A and B) and 9d.

[45] The main issues with mapping spectral features on Titan with VIMS, are 1) short exposure times especially during a fast flyby, 2) viewing geometry changes from frame to frame, and 3) dark frame subtraction that causes systematic errors in single cubes.

[46] During a typical Titan flyby, spacecraft speed and the desire to cover multiple areas, requiring fast framing, is balanced with the need for long integration times. Because only a fraction of Titan has been covered at moderately high spatial resolution (relative to the VIMS capability, < 7 km/pixel), most flybys are dedicated to coverage of more territory. Thus there are currently few image cubes that simultaneously possess spatial resolution < 7 km/pixel and long integration time ≥ 160 ms/pixel.

[47] Unlike the case for airless bodies, the viewing geometry corrections at Titan are still poorly understood. Along with light intensity changes with solar incidence angle, the amount of sunlight reaching the surface varies, and a full multiple scattering model is needed to remove the

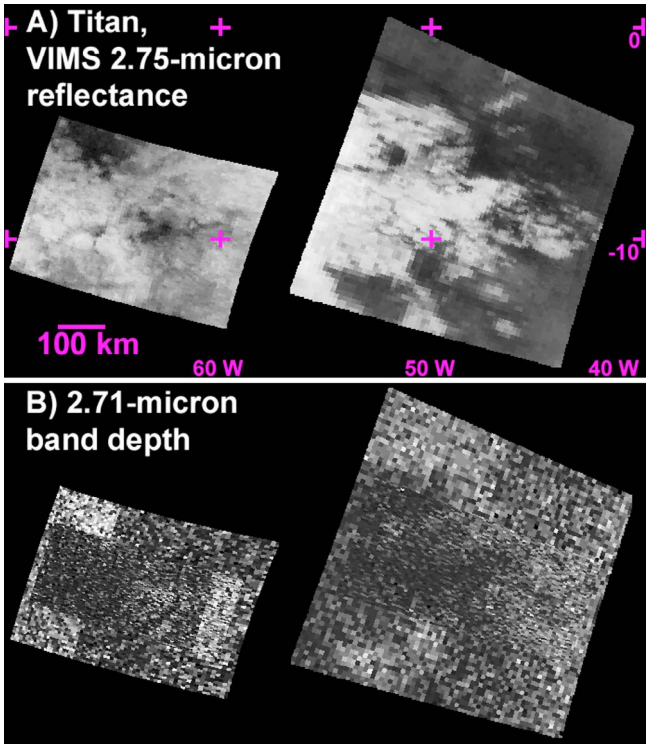

Figure 19. The same region from Figure 17 is shown for the (a) 2.75-μm reflectance and (b) 2.71-μm absorption strength. The 2.71-μm absorption shows stronger in the dark regions, another indicator of benzene.

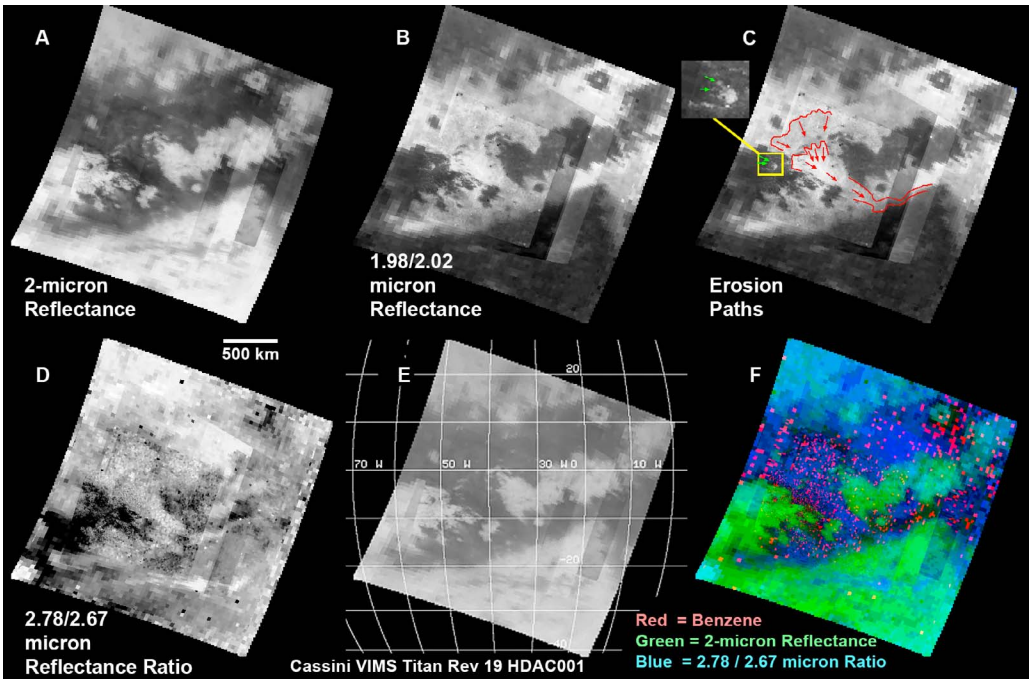

Figure 20. Titan images and spectral ratios showing larger regions of erosional features that extend over 1,700 km. Erosional processes may preferentially transport and concentrate certain compounds, like benzene.

atmospheric absorption and scattering in order to correct for lighting geometry effects.

[48] The VIMS dark subtraction can leave residual fixed pattern noise on the spectra. During the VIMS scan, data are collected across track at the programmed integration time, and on the fly back, the shutter is closed and a dark measurement is made. But the VIMS compressor only uses one dark measurement per 64 pixels. Therefore, if VIMS is framing with the ISS Narrow Angle Camera (NAC), producing 12 × 12 or 12 × 24 double resolution pixel images (these sizes match the NAC field of view), one dark spectrum is subtracted from 5 lines of 12 × 12 image data and 2.5 lines of 12 × 24 image data. Post processing, we average the 2 to 4 dark spectra and then subtract that averaged dark from every pixel in the cube. Thus the entire cube has a fixed pattern noise residual for that cube. This can cause apparent offsets and low level spectral structure, resulting in changes from cube to cube in the derived absorption band depths. This effect and the atmospheric scattering combine to make mosaics of image cubes that show significant boundaries at cube edges in the absorption band depth mapping products. One solution that we will try in the future is to use the dark measurements from nearby frames (checking for instrument temperature and voltage stability) in order to reduce the residuals.

[49] Figure 17 shows the global mapping results for three features in the 5-μm window that we have identified. Trying to ignore the offset problems described above, one sees a tendency for these features to map in darker areas. The high noise in such VIMS maps such as these led *McCord et al.* [2008] to examine the noise performance of VIMS for this problem. They found that the noise from VIMS is Gaussian in shape so that averaging pixels should reduce noise. They raised concern that spectral feature mapping algorithms could be selecting noise patterns. We analyzed the original pixels in an example cube for this effect (Figure 18). The spectral feature mapping algorithm found the pixel marked as red containing the 5.05-μm benzene-like feature, and those pixels map almost exclusively in dark regions. Block averages of the bright and dark regions show markedly different spectra with the dark region still showing the benzene feature.

[50] *McCord et al.* [2008] used the scene variance as a threshold for whether or not a feature was intense enough to be considered detected. However, the scene variance of the Titan bright and dark areas is dominated by the large reflectance level change between bright and dark regions. The criteria for detection should be instrument noise and not scene variance. Indeed, we computed the scene variance of the Cuprite, Nevada Airborne Visible and Infrared Imaging Spectrometer (AVIRIS) test scene of *Clark et al.* [2003a] and found that the scene variance was larger than many of the individual spectral features of the mapped minerals identified and confirmed with field sampling in that study. By the McCord et al. criteria, no matter how high the signal-to-noise ratio of the instrument, one could never identify compounds with an imaging spectrometer in a scene with high albedo variations. We reject such criteria as being invalid. Instead we use the statistics presented in Table 4 to determine if a detection is robust.

[51] The method of mapping compounds in VIMS data follows that described by *Clark et al.* [2003a]. Reference spectral features were continuum-removed and fitted to each pixel in the VIMS data cubes using the least squares methods. The mapping method produces 3 output images for each material: the band depth, the least squares correlation coef-

Table 4. Image Map Thresholds[a]

	Threshold DN	Threshold Band Depth Times fit (f × d)
Thresholds Used in Figure 1, Spectra S1		
Benzene 1 + 2	105	0.206
Ethane, methane	45	0.088
5.01 um band	45	0.088
Thresholds Used in Figure 3		
Benzene 1	122	0.238
Ethane, methane	88	0.172
5.01 um band	68	0.133

[a]Benzene: typical fits that correlate with the threshold f*d > 122 which corresponds to a threshold band depth × fit > = 0.238. Benzene fit values average 0.831 with a standard deviation of 0.090. DN, data number; a scaled 8-bit integer in the derived material map images. The threshold DN is the threshold level in the 8-bit image file, which corresponds to the threshold band depth in the right-most column. Benzene: Mapping found the two shapes of the 5.05-μm feature seen in Figure 2, spectra T1 and T2. The two shapes correspond to fine grained (T1) and coarse-grained (T2) benzene. Ethane, methane: maps features like that shown in Figure 2, spectrum T5. The 5.02 um band maps features like that in Figure 2, spectrum T6.

ficient (called the fit), and the weighted fit times depth. Images of the fit*depth provide the highest confidence maps and that is what is shown in the Figures 16, 17, and 18.

[52] Typical correlation coefficients (the goodness of fit) for benzene range from about 0.77 to 0.98 with a mean of ~0.85. Eight VIMS channels were used in the least squares fit when mapping benzene, so if the correlation coefficient were as low as 0.71, the probability that a feature in the spectrum of a pixel were due to noise would be 1 in 20. For fits of 0.83, the probability drops to one in 100. The average fit value in the benzene map in Figure 17b is 0.83; therefore statistically, about 1 in 100 red pixels are due to noise.

[53] The results of mapping the 4.97-, 5.01- and 5.05-μm absorption features are shown in Figure 16 (middle). While many of the cubes used to make the mosaic are those with shorter integration times, there is a tendency to map more pixels in dark regions. If benzene is present, there should also be an absorption in the 2.71-μm region. VIMS detects this absorption at a single channel, and Figure 16 (bottom) shows the 2.71-μm single channel relative absorption strength. The 2.71-μm feature map shows greater strength in dark regions, particularly in the regions of the H-shaped dark area, called Fensal-Aztlan, where the same area shows strong 5.05-μm absorption bands.

[54] Figure 17 shows where the strongest 4.97-, 5.01-, and 5.05-μm absorptions map in the high spatial resolution, long integration time VIMS cubes. Not only do the organic absorption bands in this region map in the dark terrain, the 2.78/2.68-μm reflectance ratio (Figure 17c) is high, indicating water cannot explain the spectral shape (as indicated in Figure 11), even if we correct the ratio, lowering it by 1.1× due to atmospheric absorption. The 2.78/2.68-μm reflectance ratio is > 1 everywhere in these images, and for atmospherically corrected data would be > 0.9 except for location d (Figure 17c), where the ratio is about 0.8. There are only a few small locations detected on Titan to date in the VIMS images with the ratio this low.

[55] The presence of benzene should also have indicators in the 2.71-μm region. Indeed, Figure 19 shows that the 2.71-μm absorption band depresses the reflectance at that wavelength. This depression is illustrated in the spectra in Figure 9f for the benzene "lake" in Figure 17b, location a, which also shows as a bright spot in Figure 19b.

[56] Moving out and examining lower spatial resolution, long integration time cubes, the same trends are mapped as shown in Figure 20. But this larger view may reveal why benzene tends to show in greater concentration in this region (besides the fact that the VIMS data have higher signal-to-noise ratio in this area): vast erosion processes have shaped this region. Evidence for erosion has been previously reported by *Jaumann et al.* [2008]. Some reflectance ratios reveal subtle details that are not as apparent in reflectance or in ratios of reflectances from other windows. For example the ratio within a window, 2.78/2.68-μm reflectance ratio, shows subtle detail in dark regions (Figure 20b). If Titan's surface were exposed water ice, this ratio would be quite flat with essentially no spectral structure. The fact that this ratio shows strong contrast indicates highly variable spectral slopes across this narrow spectral range, typical of many organic compounds, but not water ice.

7. North Polar Hood and HCN Cloud

[57] It has been known since the Voyager flyby that Titan's north polar region develops a cloud of HCN gas during northern winter [e.g., *Coustenis et al.*, 1999, 2006; *Samuelson et al.*, 2007, and references therein]. VIMS, too, has detected an aerosol cloud of HCN (Figures 21a and 21b). This cloud has unusual spectral properties in the VIMS data showing the classic Christenson response of light reflecting specularly from particulate surfaces (Figure 21b). In order to have this response, the particles must be larger than the 5-μm wavelengths probing the cloud. INMS [*Waite et al.*, 2007; *Samuelson et al.*, 2007] also found large particles in the upper atmosphere, adding to the evidence of high altitude aerosols with complex chemistry. *Samuelson et al.* [2007] found absorptions in Cassini CIRS data consistent with HCN ice less than or equal to 5 microns and the VIMS data also confirm this.

[58] The spectrum of HCN was measured in the laboratory for the comparison in Figure 21. Due to safety considerations, 2 g of HCN were synthesized and kept at a low temperature in order to keep the vapor pressure as safe as reasonable. At a temperature of 82K, the HCN remained as a sticky malleable substance. The HCN would stick to a Teflon spatula. This indicates that on Titan, HCN aerosols would stick together and possibly with other molecules, and grow until they were large enough to fall to the surface. While HCN is most abundant (as measured by Voyager and Cassini) at the northern winter pole, HCN exists in Titan's atmosphere over the whole moon [*Coustenis et al.*, 2006]. Thus, HCN and other polar organic molecules may play a role in the creation of large aerosols and delivering them to the surface.

[59] Because HC_3N is a possible explanation for Titan's 4.91-μm spectral feature (Figure 9d), it may indicate that HCN gets modified to HC_3N. HC_3N spectra are consistent with Titan's bright material, but higher spectral resolution data are required to confirm this possibility.

8. Discussion

[60] Both acetylene and benzene should be produced from methane by photochemical processes in Titan's upper

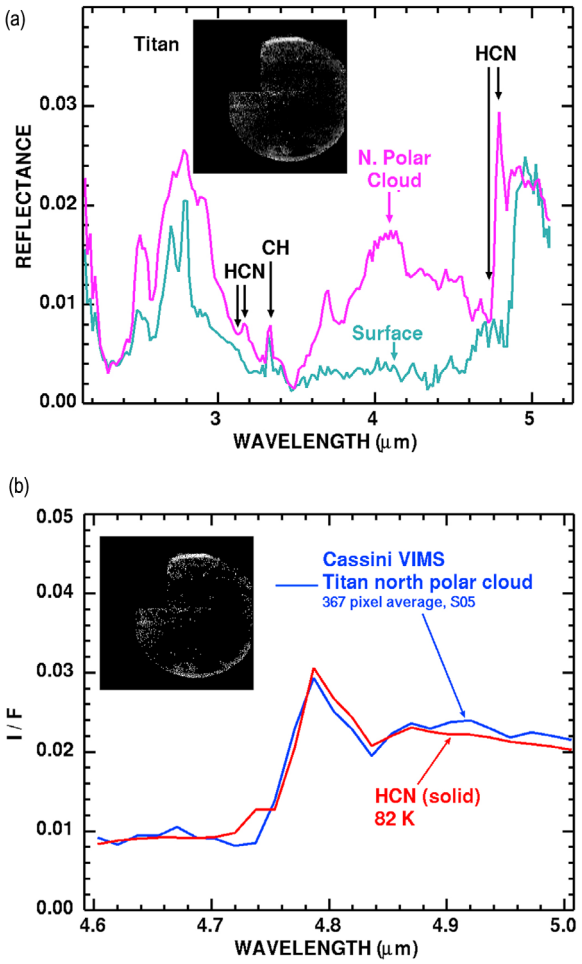

Figure 21. (a) Titan polar cloud as observed by VIMS and spectra of the cloud. The HCN spectral structure indicated by the arrows matches the index of refraction spectra (and Christensen frequencies) of solid HCN and are not gas emission lines. The arrow pointing to the CH peak is an emission line from gaseous methane. (b) The Titan polar spectrum, when compared to solid HCN, indicates that large particles of solid HCN exist in the observed cloud. The peak is not a gas emission line; it is the peak in the solid or liquid HCN index of refraction. The aerosol particles must be similar to or larger than the wavelength of light at the 5-μm wavelength used.

atmosphere and incorporated into aerosols by condensation and growth to eventually fall to the surface. Recent photochemical models [e.g., *Vuitton et al.*, 2006, 2008, and references therein] predict a net (production minus loss) creation of acetylene approximately 125–2000 times larger than that of benzene [*Wilson and Atreya*, 2004] consistent with Earth-based infrared observations of Titan's atmosphere [*Coustenis et al.*, 2003] and Cassini CIRS observations [*Coustenis et al.*, 2006] which set the acetylene/benzene ratio at 2000 to 10,000. Once aerosols form, they carry the condensates to the surface, which is well-shielded from ultraviolet radiation. Thus, we would expect from these models that the surface acetylene-to-benzene ratio should be that determined by the stratospheric photochemistry. *Vuitton et al.* [2008] predict surface acetylene to be 125 times that of benzene. However, the Cassini INMS, directly sampling the thermosphere found the acetylene/benzene ratio to be much lower, ~36 [*Waite et al.*, 2007]. *Vuitton et al.* [2008] show that some of the benzene signal seen by the INMS can be explained by recombination of phenyl radicals ($C_6H_5^+$) with H atoms on the walls of the instrument. They present models that indicate benzene is efficiently produced by ion chemistry in the upper atmosphere but would be quickly photolyzed in the ionosphere leading to downward diffusions of complex aromatic species. Their model indicates an accumulated surface layer of ~3 m of solid aromatic hydrocarbons, including a ~20 cm benzene thickness.

[61] The VIMS data indicate the surface acetylene/benzene abundance probably cannot be greater than about 10. The laboratory spectra of acetylene, benzene and each of their mixtures with added carbon black, to lower reflectances to that typical of Titan's surface (Figure 9), suggest that the acetylene/benzene ratio $\ll$1. Further, reflectance through Titan's 2.68 and 2.78-μm windows is sensitive to absorptions in that spectral region. Acetylene has the 2.78/2.68 μm reflectance ratio <1 whereas Titan has most of its surface reflectance ratio >1 (Table 2), similar to that of benzene. We detect no acetylene in any VIMS data, from either its absorption in the 5-μm region, or in the 2.68 and 2.78-μm windows, and set conservative abundance limits on acetylene of <10%. Benzene maps in small outcrops, where the benzene abundance is tens of percent for the observed band depths of 30% to 40%. If the benzene were fine grained, close to 100% abundance would be required to explain the observed band depths and benzene/acetylene <1 in those outcrops. Benzene was detected in about 20% of VIMS pixels for the VIMS data having sufficient integration time and high spatial resolution. Assuming this is a representative value for global benzene, and each pixel contains a conservative estimate of 20% benzene, global benzene would be about 4% in the optical surface. Because the areas where VIMS mapped high benzene includes significant dark regions near the equator, we reduce the abundance by another factor of 4 because most of Titan contains brighter regions where little benzene is detected in VIMS data. With an acetylene surface abundance <10% and benzene ~1%, we derive a conservative value of acetylene/benzene < ~10. This surface result, along with the similar INMS result of 36, which indicates that benzene is very abundant in the thermosphere [*Waite et al.*, 2007] if all of the INMS benzene signal is real, it means that the mechanism creating benzene is more active on Titan than previously thought. Additional evidence for benzene is indicated by the 2.78/2.68 μm reflectance ratio. This ratio remains above 1 for almost all of Titan's surface, and is slightly higher in dark areas where benzene maps (Figures 16, 17, and 19), with values similar to benzene (Table 2).

[62] Possible mechanisms for altering the ratio of these two hydrocarbons on the surface are considered in turn: (1) chemical conversion of acetylene to benzene aided by radiolysis from cosmic rays; (2) spontaneous conversion at the surface of acetylene to benzene; (3) preferential transport of one or the other hydrocarbon so as to render the benzene more exposed to remote sensing detection; and (4) sequestering acetylene in the subsurface. Mechanism 1 is plausible,

since formation pathways for benzene begin with acetylene, in concert with other hydrocarbon radicals [*Wilson et al.*, 2003]. Although the UV energy flux at Titan's surface is zero, some cosmic rays incident at the top of the atmosphere reach Titan's surface, and may convert a portion of the acetylene surface deposits into other compounds such as benzene. The amount of energy deposited by cosmic rays in the atmosphere is less than that of solar ultraviolet radiation by a factor of several to perhaps 10 [*Bernard*, 2004], and the amount available at the surface relative to the peak deposition at about 50 km altitude is down by another factor of a few [*Sagan et al.*, 1992]. It therefore seems unlikely that 99% of the acetylene could be converted to benzene by the available flux of energy at the surface. However, the possibility of conversion in the atmosphere during aerosol sedimentation by cosmic rays and longer wavelength ultraviolet light (acetylene is more readily dissociated by longer wavelength UV than is methane) should be examined more closely. The high abundance of benzene observed by INMS [*Waite et al.*, 2007] supports the interpretation that benzene is created high in Titan's atmosphere and that previous estimates of benzene conversion rates may be too low. Indeed, the increased production of benzene by radiolysis from cosmic rays appears to be a major discovery by Cassini INMS measurements [*Waite et al.*, 2007], although some of the benzene signal appears to be created in the INMS instrument [*Vuitton et al.*, 2008] as already noted. Nevertheless, the high benzene abundance relative to acetylene in Titan's thermosphere indicates that the conversion from methane rapidly proceeds past acetylene, thus driving high production of benzene in the atmosphere relative to what is predicted by current models.

[63] Mechanism 2 is plausible because acetylene can cyclize into benzene under the action of high temperature, energizing radiation or the presence of catalytic surfaces [*Rucker et al.*, 1986]. High temperatures (>176 K) are possible during cryovolcanic events involving water or water ammonia fluids; hypervelocity impacts briefly create much higher temperatures and acetylene conversion to more stable forms is virtually guaranteed in such events. Spontaneous formation after surface disturbance by methane rainfall and runoff, perhaps exposing fresh catalytic surfaces to acetylene-rich sediments being transported by the liquid, is also possible but more speculative. Once formed, benzene is stable in the Titan environment and should not polymerize into other forms.

[64] Mechanism 3 relies on the potential difference in the material properties of solid acetylene (melting point 192 K) versus benzene (melting point 267 K) at 94 K to create different mean particle sizes and hence different aeolian transport properties. *Lorenz et al.* [2006] suggest the dunes observed by Cassini radar are sand-sized particles aggregated from smaller aerosol deposits. It is possible, particularly if acetylene is further processed on the surface into benzene and/or linear polymers of various types, that aeolian sorting of particle sizes also sorts and segregates acetylene from benzene, leading to concentration gradients over spatially resolvable scales. Absent detailed information on the rheological properties of these materials at 94K, and the specific setting in which the photochemical aerosols are deposited, we suggest this as a possibility but do not pursue it further. Note that while VIMS detects benzene in areas of dunes, it is only one of the compounds comprising the dunes and more data are needed to determine the other components.

[65] Mechanism 4, hiding acetylene below the surface, is possible but unlikely. Titan's surface shows extensive fluvial action, including erosion through channels [*Tomasko et al.*, 2005; *Lorenz et al.*, 2006; *Jaumann et al.*, 2008] and possible modification by cryovolcanism [*Sotin et al.*, 2005]. Erosional processes tend to expose, transport and concentrate material, so one would expect acetylene deposits to be exposed and detectable, either from the 5-μm absorption, or from a low 2.78/2.68 μm reflectance ratio. Also, it is difficult to understand why such processes would preferentially bury acetylene relative to benzene.

[66] The areal distribution of benzene is consistent with erosional processes and subsequent concentration. In the highest resolution VIMS data (Figures 17 and 20), benzene is more prevalent in channels, at the bright/dark terrain boundaries (where erosional processes are likely maximum), and in what appear to be small "lakes" (round dark areas). The following is one scenario for this distribution pattern. The compounds that are formed in the thermosphere and observed by INMS are transported down into the stratosphere where they appear to complex into aerosol compounds [*Waite et al.*, 2007] before precipitating on the surface to be observed by VIMS. Precipitating into aerosols removes/reduces the compound from the atmosphere vapor phase so atmospheric instruments like Cassini CIRS would see reduced gas abundance, reconciling the high INMS and VIMS benzene results with CIRS detection of low benzene gas in the atmosphere (with additional complications of the INMS instrument partly manufacturing the benzene signal, as already discussed). However, additional surface enhancement or enrichment of benzene relative to acetylene is still required to explain the high benzene abundance detected by VIMS relative to the current photochemical models.

[67] A methane + ethane rain may mix with a surface coating of hydrocarbons and nitriles to produce an organic-rich slurry that is preferentially removed from the bright highlands to accumulate in channels and lakes, at the base of slopes, and on low-lying plains. These low-lying plains may remain muddy at or just below the surface, as indicated at the Huygens landing site and more extensively in the VIMS data. Erosional processes initially concentrate certain compounds like benzene, followed by later erosional processes that expose those accumulated deposits of benzene and other organic compounds. This implies a dynamic surface with a continued history of erosion and deposition.

[68] In addition to numerous sinuous channels, Figure 17c shows an anomalous area on Titan where the 2.78/2.68 μm reflectance ratio is less than one. The low ratio (0.9 to 1) shows a diffuse dark cloud in Figure 17c, which has a concentration of alkanes (Figure 17d). Ethane has a high 2.78/2.68 ratio, but thin layers (~1 mm) of methane liquid has 2.78/2.68 ratios <1 (Figures 13a, 13b, Table 2). Trace amounts of ammonia or water could also drive the ratio below 1, because only low abundances are allowed as the ratios for those materials are significantly less than 0.5 at high abundances (Figure 11 and Table 2). The apparent source area is dark and circular with what may be flow channels extending away from the source region, Figure 17e. This area may be an impact ejecta blanket that was distributed in the diffuse pattern, or a cryo-volcanic center spewing material hundreds of

km. Reflectance images show no indication of crater morphology, leading to a local geyser or volcanic activity as a plausible explanation. RADAR shows that the VIMS-dark feature is a positive topographic edifice, which does not favor the impact ejecta blanket but rather the cryovolcanic center [*Barnes et al.*, 2007b].

[69] The conclusion from this study regarding detection of *liquid* hydrocarbons is that VIMS is only sensitive to quantifying small path lengths in liquid methane or ethane and all light gets absorbed at shorter and shorter wavelengths as the path length increases. For clear lakes deeper than 3 cm, VIMS would detect essentially no light at 2.0, 2.7, and 5 μm, and a search of VIMS data has to date failed to find any locations on Titan larger than a pixel with those spectral properties. At clear lake depths >0.1 m (path length >0.2 m) essentially all light would be absorbed in all the VIMS windows. VIMS could not detect sub-pixel >0.1-m deep clear lakes on Titan, as they would only lower the apparent reflectance and provide no information for detection. Specular reflection of surface liquids from diffuse scattering off of aerosols in the atmosphere complicate these signals at wavelengths shorter than about 2 μm, especially at low solar incidence angles in the polar regions. Such reflections would add apparent signals to the observed spectra that would normally be black due to absorption by those liquids. Such scattering and reflection needs to be considered when determining lake depths.

[70] While many organic compounds have now been detected in the atmosphere and on Titan's surface, we still have only a small spectral database of organic compounds to compare to spectra of Titan. Spectra of additional compounds are needed, along with higher spatial and spectral resolution data on Titan's surface in order to better understand the full compositional range of compounds on Titan.

[71] **Acknowledgments.** This study was funded by the NASA Cassini project, VIMS team, and Cassini Data Analysis program (R. Clark, PI). This work was financed within the scope of the program "Incentivazione alla mobilita' di studiosi straineri e italiani residenti all'estero."

References

Anderson, C. M., R. E. Samuelson, G. L. Bjoraker, and R. K. Achterberg (2010), Particle size and abundance of HC_3N ice in Titan's lower stratosphere at high northern latitudes, *Icarus*, *207*, 914–922, doi:10.1016/j.icarus.2009.12.024.

Anderson, G., et al. (2006), Atmospheric sensitivity to spectral top-of-atmosphere solar irradiance perturbations, using MODTRAN-5 Radiative Transfer Algorithm, *Eos Trans. AGU*, *87*(52), Fall Meet. Suppl., Abstract A11C–05.

Barnes, J. W., et al. (2005), A 5-μm bright spot on Titan: Evidence for surface diversity, *Science*, *310*, 92–95, doi:10.1126/science.1117075.

Barnes, J. W., R. H. Brown, L. Soderblom, B. J. Buratti, C. Sotin, S. Rodriguez, S. Le Mouélic, K. H. Baines, R. Clark, and P. Nicholson (2007a), Global-scale surface spectral variations on Titan seen from Cassini/VIMS, *Icarus*, *186*, 242–258, doi:10.1016/j.icarus.2006.08.021.

Barnes, J. W., et al. (2007b), Near-infrared spectral mapping of Titan's mountains and channels, *J. Geophys. Res.*, *112*, E11006, doi:10.1029/2007JE002932.

Barnes, J. W., et al. (2008), Spectroscopy, morphometry, and photoclinometry of Titans dunefields from Cassini/VIMS, *Icarus*, *195*, 400–414, doi:10.1016/j.icarus.2007.12.006.

Barnes, J. W., et al. (2009), Shoreline features of Titan's Ontario Lacus from Cassini/VIMS observations, *Icarus*, *201*, 217–225, doi:10.1016/j.icarus.2008.12.028.

Bates, R. L., and J. A. Jackson (Eds.) (1976), *Dictionary of Geologic Terms*, 290 pp., Anchor Press, Garden City, New York.

Bellucci, A., B. Sicardy, P. Drossart, P. Rannou, P. D. Nicholson, M. Hedman, K. H. Baines, and B. Burrati (2009), Titan solar occultation observed by *Cassini*/VIMS: Gas absorption and constraints on aerosol composition, *Icarus*, *201*, 198–216, doi:10.1016/j.icarus.2008.12.024.

Bernard, M. J.-M. (2004), Experimental simulation of the Titan's atmospheric chemistry: study of the reaction products and comparison with a kinetic model, Ph.D. thesis, 234 pp., Universite Paris 7, Paris.

Boudon, V., J.-P. Champion, T. Gabard, M. Loëte, F. Michelot, G. Pierre, M. Rotger, C. Wenger, and M. Rey (2004), Symmetry-adapted tensorial formalism to model rovibrational and rovibronic spectra of molecules pertaining to various point groups, *J. Mol. Spectrosc.*, *228*, 620–634, doi:10.1016/j.jms.2004.02.022.

Brown, R. H., et al. (2004), The Cassini visual and infrared mapping spectrometer investigation, *Space Sci. Rev.*, *115*(1–4), 111–168, doi:10.1007/s11214-004-1453-x.

Brown, R. H., L. A. Soderblom, J. M. Soderblom, R. N. Clark, R. Jaumann, J. W. Barnes, C. Sotin, B. Buratti, K. H. Baines, and P. D. Nicholson (2008), The identification of liquid ethane in Titan's Ontario Lacus, *Nature*, *454*, 607–610, doi:10.1038/nature07100.

Clark, R. N., G. A. Swayze, K. E. Livo, R. F. Kokaly, S. J. Sutley, J. B. Dalton, R. R. McDougal, and C. A. Gent (2003a), Imaging spectroscopy: Earth and planetary remote sensing with the USGS Tetracorder and expert systems, *J. Geophys. Res.*, *108*(E12), 5131, doi:10.1029/2002JE001847.

Clark, R. N., G. A. Swayze, R. Wise, E. Livo, T. Hoefen, R. Kokaly, and S. J. Sutley (2003b), USGS digital spectral library splib05a, *U.S. Geological Surv. Open File Rep.*, *03–395*.

Clark, R. N., et al. (2005), Compositional maps of Saturn's moon Phoebe from imaging spectroscopy, *Nature*, *435*, 66–69, doi:10.1038/nature03558.

Clark, R. N., G. A. Swayze, R. Wise, E. Livo, T. Hoefen, R. Kokaly, and S. J. Sutley (2007), USGS digital spectral library splib06a, *U.S. Geol. Surv. Digital Data Ser. 231*.

Clark, R. N., et al. (2008), Compositional mapping of Saturn's satellite Dione with Cassini VIMS and implications of dark material in the Saturn system, *Icarus*, *193*, 372–386, doi:10.1016/j.icarus.2007.08.035.

Clark, R. N., J. M. Curchin, T. M. Hoefen, and G. A. Swayze (2009), Reflectance spectroscopy of organic compounds: 1. Alkanes, *J. Geophys. Res.*, *114*, E03001, doi:10.1029/2008JE003150.

Coustenis, A. (2005), Formation and evolution of Titan's atmosphere, *Space Sci. Rev.*, *116*, 171–184, doi:10.1007/s11214-005-1954-2.

Coustenis, A., B. Bezard, and D. Gautier (1989), Titan's atmosphere from Voyager integrated observations–II. The CH_3D abundance and D/H ration from the 900–1200 cm^{-1} spectral region, *Icarus*, *82*, 67–80, doi:10.1016/0019-1035(89)90024-9.

Coustenis, A., E. Lellouch, J.-P. Maillard, and C. P. McKay (1995), Titan's surface: Composition and variability from the near-infrared albedo, *Icarus*, *118*, 87–104, doi:10.1006/icar.1995.1179.

Coustenis, A., B. Schmitt, R. Khanna, and F. Trotta (1999), Plausible condensates in Titan's stratosphere from Voyager infrared spectra, *Planet. Space Sci.*, *47*, 1305–1329, doi:10.1016/S0032-0633(99)00053-7.

Coustenis, A., A. Salama, B. Schultz, S. Ott, E. Lellouch, T. Encrenaz, D. Gautier, and H. Feuchtgruber (2003), Titan's atmosphere from ISO mid-infrared spectroscopy, *Icarus*, *161*, 383–403, doi:10.1016/S0019-1035(02)00028-3.

Coustenis, A., et al. (2006), Titan's 3-μm spectral region from ISO high-resolution spectroscopy, *Icarus*, *180*, 176–185, doi:10.1016/j.icarus.2005.08.007.

Coustenis, A., et al. (2007), The composition of Titan's stratosphere from Cassini/CIRS mid-infrared spectra, *Icarus*, *189*, 35–62, doi:10.1016/j.icarus.2006.12.022.

Coustenis, A., et al. (2008), Detection of C_2HD and the D/H ratio on Titan, *Icarus*, *197*, 539–548, doi:10.1016/j.icarus.2008.06.003.

DeKok, R., et al. (2007), Oxygen compounds in Titan's stratosphere as observed by Cassini CIRS, *Icarus*, *186*, 354–363, doi:10.1016/j.icarus.2006.09.016.

Elachi, C., et al. (2005), Cassini radar views the surface of Titan, *Science*, *308*, 970–974, doi:10.1126/science.1109919.

Flasar, F. M., et al. (2005), Titan's atmospheric temperatures, winds, and composition, *Science*, *308*, 975–978, doi:10.1126/science.1111150.

Fulchignoni, M., et al. (2005), In situ measurements of the physical characteristics of Titan's environment, *Nature*, *438*, 785–791, doi:10.1038/nature04314.

Griffith, C. A. (1993), Evidence for surface heterogeneity on Titan, *Nature*, *364*, 511–514, doi:10.1038/364511a0.

Griffith, C. A., T. Owen, T. Geballe, J. Rayner, and P. Rannou (2003), Evidence for the exposure of water ice on Titan's surface, *Science*, *300*, 628–630, doi:10.1126/science.1081897.

Griffith, C. A., et al. (2005), The evolution of Titan's mid-latitude clouds, *Science*, *310*, 474–477, doi:10.1126/science.1117702.

Griffith, C. A., P. Penteado, S. Rodriguez, S. Le Mouélic, K. H. Baines, B. Buratti, R. Clark, P. Nicholson, R. Jaumann, and C. Sotin (2009), Characterization of clouds in Titan's tropical atmosphere, *Astrophys. J.*, *702*, L105–L109, doi:10.1088/0004-637X/702/2/L105.

Hudson, C. M., and R. K. Khanna (1987), Absolute intensities and complex refractive indices of crystalline HC3N in the infrared region, paper presented at the 42nd Symposium on Molecular Spectroscopy, Columbus, Ohio.

Irwin, P. G. J., L. A. Sromovsky, E. K. Strong, K. Sihra, N. A. Teanby, N. Bowles, S. B. Calcutt, and J. J. Remedios (2006), Improved near-infrared methane band models and k-distribution parameters from 2000 to 9500 cm^{-1} and implications for interpretation of outer planet spectra, *Icarus*, *181*, 309–319, doi:10.1016/j.icarus.2005.11.003.

Israel, G., et al. (2005), Complex organic matter in Titan's atmospheric aerosols from in situ pyrolysis and analysis, *Nature*, *438*, 796–799, doi:10.1038/nature04349.

Janssen, M. A., et al. (2009), Titan's surface at 2.2-cm wavelength imaged by the Cassini Radar radiometer: Calibration and first results, *Icarus*, *200*, 222–239, doi:10.1016/j.icarus.2008.10.017.

Jaumann, R., et al. (2008), Fluvial erosion and post-erosional processes on Titan, *Icarus*, *197*, 526–538, doi:10.1016/j.icarus.2008.06.002.

Jaumann, R., et al. (2006), High resolution CASSINI-VIMS mosaics of Titan and the icy Saturnian satellites, *Planet. Space Sci.*, *54*, 1146–1155, doi:10.1016/j.pss.2006.05.034.

Khanna, R. K. (2005), Condensed species in Titan's stratosphere: Confirmation of crystalline cyanoacetylene (HC3N) and evidence for crystalline acetylene (C2 H2) on Titan, *Icarus*, *178*, 165–170, doi:10.1016/j.icarus.2005.03.011.

Khare, B. N., C. Sagan, E. T. Arakawa, F. Suits, T. A. Callcott, and M. W. Williams (1984), Optical constants of organic tholins produced in a simulated titanian atmosphere: From soft X-ray to microwave frequencies, *Icarus*, *60*, 127–137, doi:10.1016/0019-1035(84)90142-8.

Lellouch, E., A. Coustenis, B. Sebag, J.-G. Cuby, M. Lopez-Valverde, B. Schmitt, T. Fouchet, and J. Crovisier (2003), Titan's 5-μm window: Observations with the very large telescope, *Icarus*, *162*, 125–142, doi:10.1016/S0019-1035(02)00079-9.

Lellouch, E., B. Schmitt, A. Coustenis, and J.-G. Cuby (2004), Titan's 5-μm lightcurve, *Icarus*, *168*, 209–214, doi:10.1016/j.icarus.2003.12.001.

Lemmon, M. T., E. Karkoshka, and M. Tomasko (1993), Titan's rotation: Surface feature observed, *Icarus*, *103*, 329–332, doi:10.1006/icar.1993.1074.

Lemmon, M. T., E. Karkoshka, and M. Tomasko (1995), Titan's rotational lightcurve, *Icarus*, *113*, 27–38, doi:10.1006/icar.1995.1003.

Le Mouélic, S., et al. (2008), Mapping and interpretation of Sinlap crater on Titan using Cassini VIMS and RADAR data, *J. Geophys. Res. 113*, E04003, doi:10.1029/2007JE002965.

Lorenz, R. D., et al. (2006), The sand seas of Titan: Cassini RADAR observations of longitudinal dunes, *Science*, *312*, 724–727, doi:10.1126/science.1123257.

Marten, A., T. Hidayat, Y. Biraud, and R. Moreno (2002), New millimeter heterodyne observations of Titan: Vertical distributions of nitriles, HCN, HC_3N, CH_3CN and the Isotopic $^{15}N/^{14}N$ in its atmosphere, *Icarus*, *158*, 532–544, doi:10.1006/icar.2002.6897.

McCord, T. B., et al. (2006), Composition of Titan's surface from Cassini VIMS, *Planet. Space Sci.*, *54*, 1524–1539, doi:10.1016/j.pss.2006.06.007.

McCord, T. B., et al. (2008), Titan's surface: Search for spectral diversity and composition using the Cassini VIMS investigation, *Icarus*, *194*, 212–242, doi:10.1016/j.icarus.2007.08.039.

McKellar, A. R. W. (1989), The spectrum of gaseous methane at 77 K in the 1.1–2.6-micron region: A benchmark for planetary astronomy, *Can. J. Phys.*, *67*, 1027–1035.

Nelson, R. M., et al. (2009), Saturn's Titan: Surface change, ammonia, and implications for atmospheric and tectonic activity, *Icarus*, *199*, 429–441, doi:10.1016/j.icarus.2008.08.013.

Niemann, H. B., et al. (2005), The abundance of constituents of Titan's atmosphere from the GCMS instrument on the Huygens probe, *Nature*, *438*, 779–784, doi:10.1038/nature04122.

Rannou, P., T. Cours, S. Le Mouélic, S. Rodriguez, C. Sotin, P. Drossart, and R. Brown (2010), Titan haze distribution and optical properties retrieved from recent observations, *Icarus*, *208*, 850–867, doi:10.1016/j.icarus.2010.03.016.

Rodriguez, S., et al. (2006), Cassini/VIMS hyperspectral observations of the HUYGENS landing site on Titan, *Planet. Space Sci.*, *54*, 1510–1523, doi:10.1016/j.pss.2006.06.016.

Rodriguez, S., et al. (2009), Fast forward modeling of Titan's infrared spectra to invert hyperspectral images acquired by the VIMS instrument onboard Cassini-Huygens, paper presented at Workshop on Hyperspectral Image and Signal Processing: Evolution in Remote Sensing (Whispers), Inst. of Electr. and Electr. Eng., Grenoble, France, 26–28 Aug.

Rucker, T. G., M. A. Logan, T. M. Gentle, E. L. Muetterties, and G. A. And Somorjai (1986), Conversion of acetylene to benzene over palladium single-crystal surfaces: 1. The low-pressure stoichiometric and the high-pressure catalytic reactions, *J. Phys. Chem.*, *90*, 2703–2708, doi:10.1021/j100403a029.

Sagan, C., W. R. Thompson, and B. Khare (1992), Titan: A laboratory for pre-bological organic chemistry, *Acc. Chem. Res.*, *25*, 286–292, doi:10.1021/ar00019a003.

Samuelson, R. E. (1985), Clouds and aerosols in Titan's atmosphere, *ESA Spec. Pap.*, *241*, 99–107.

Samuelson, R. E. (1992), Infrared properties of Titan's clouds and aerosols, *ESA Spec. Pap.*, *338*, 191–195.

Samuelson, R. E., M. D. Smith, R. K. Achterberg, and J. C. Pearl (2007), Cassini CIRS update on stratospheric ices at Titan's winter pole, *Icarus*, *189*, 63–71, doi:10.1016/j.icarus.2007.02.005.

Schroeder, S. E., and H. U. Keller (2008), The reflectance spectrum of Titan's surface at the Huygens landing site determined by the descent imager/spectral radiometer, *Planet. Space Sci.*, *56*, 753–769, doi:10.1016/j.pss.2007.10.011.

Soderblom, L. A., J. W. Barnes, R. H. Brown, R. N. Clark, M. A. Janssen, T. B. McCord, H. B. Niemann, and M. G. Tomasko (2009), Composition of Titan's surface, in *Titan from Cassini-Huygens*, edited by R. H. Brown et al., chap. 6, pp. 141–175, Springer, New York.

Sotin, C., et al. (2005), Release of volatiles from a possible cryovolcano from near-infrared imaging of Titan, *Nature*, *435*, 786–789, doi:10.1038nature03596.

Teanby, N. A., P. G. J. Irwin, R. de Kok, A. Jolly, B. Bezard, C. A. Nixon, and S. B. Calcutt (2009), Titan's stratospheric C_2N_2, C_3H_4, and C_4H_2 abundances from Cassini/CIRS far-infrared spectra, *Icarus*, *202*, 620–631, doi:10.1016/j.icarus.2009.03.022.

Tomasko, M. G., et al. (2005), Rain, wind and haze during the Huygens probe's descent to Titan's surface, *Nature*, *438*, 765–778, doi:10.1038/nature04126.

Tomasko, M. G., B. Bézard, L. Doose, S. Engel, and E. Karkoschka (2008a), Measurements of methane absorption by the descent imager/spectral radiometer (DISR) during its descent through Titan's atmosphere, *Planet. Space Sci.*, *56*, 624–647, doi:10.1016/j.pss.2007.10.009.

Tomasko, M. G., L. Doose, S. Engel, L. E. Dafoe, R. West, M. Lemmon, E. Karkoschka, and C. See (2008b), A model of Titan's aerosols based on measurements made inside the atmosphere,*Planet. Space Sci.*, *56*, 669–707, doi:10.1016/j.pss.2007.11.019.

Vuitton, V., J.-F. Doussin, Y. Bénilan, F. Raulin, and M.-C. Gazeau (2006), Experimental and theoretical study of hydrocarbon photochemistry applied to Titan stratosphere, *Icarus*, *185*, 287–300, doi:10.1016/j.icarus.2006.06.002.

Vuitton, V., R. V. Yelle, and J. Cui (2008), Formation and distribution of benzene on Titan, *J. Geophys. Res.*, *113*, E05007, doi:10.1029/2007JE002997.

Waite, J. H., et al. (2005), Ion neutral mass spectrometer results from the first flyby of Titan, *Science*, *308*, 982–986, doi:10.1126/science.1110652.

Waite, H., D. Young, T. Cravens, A. Coates, F. Crary, B. Magee, and J. Westlake (2007), The Process of Tholin Formation in Titan's Upper Atmosphere, *Science*, *316*, 870–875, doi:10.1126/science.1139727.

Wilson, E. H., and S. K. Atreya (2004), Current state of modeling the photochemistry of Titan's mutually dependent atmosphere and ionosphere, *J. Geophys. Res.*, *109*, E06002, doi:10.1029/2003JE002181.

Wilson, E. H., S. K. Atreya, and A. Coustenis (2003), Mechanisms for the formation of benzene in the atmosphere of Titan, *J. Geophys. Res.*, *108*(E2), 5014, doi:10.1029/2002JE001896.

Wye, L., H. Zebker, S. Ostro, R. West, Y. Gim, R. Lorenz, and the Cassini RADAR Team (2007), Electrical properties of Titan's surface from Cassini RADAR scatterometer measurements, *Icarus*, *188*, 367–385, doi:10.1016/j.icarus.2006.12.008.

Yung, Y. L., and W. B. DeMore (1999), *Photochemistry of Planetary Atmospheres*, 456 pp., Oxford Univ. Press, New York.

Zebker, H., L. Wye, M. Janssen, and the Cassini RADAR Team (2008), Titan's surface from reconciled Cassini microwave reflectivity and emissivity observations, *Icarus*, *194*, 704–710, doi:10.1016/j.icarus.2007.10.019.

K. H. Baines, B. J. Buratti, and C. Sotin, Jet Propulsion Laboratory, Mail Stop 183-501, 4800 Oak Grove Dr., Pasadena, CA 91109, USA.

J. W. Barnes, Department of Physics, University of Idaho, Box 440903, Moscow, ID 83844, USA.

R. H. Brown, Lunar and Planetary Laboratory, Department of Planetary Sciences, University of Arizona, 1629 East University Blvd., Tucson, AZ 85721, USA.

R. N. Clark, J. M. Curchin, and T. M. Hoefen, U.S. Geological Survey, Mail Stop 964, Box 25046, Denver Federal Center, Denver, CO 80225, USA. (rclark@usgs.gov)

D. P. Cruikshank, Astrophysics Branch, NASA Ames Research Center, Mail Stop 245-6, Moffett Field, CA 94035, USA.

R. Jaumann and K. Stephan, Institute of Space Sensor Technology and Planetary Exploration, German Aerospace Center, Berlin, Rutherfordstrasse 2, D-12489 Berlin, Germany.

S. Le Mouélic, Laboratoire de Planétologie et Géodynamique, UMR 6112, Université de Nantes, CNRS, 2 rue de la Houssinière, F-44000 Nantes, France.

J. Lunine, Department of Physics, University of Rome Tor Vergata, I-00133 Roma, Italy.

P. D. Nicholson, Department of Astronomy, Cornell University, 418 Space Sciences Bldg., Ithaca, NY 14853, USA.

S. Rodriguez, Laboratoire AIM, Université Paris 7, CNRS, CEA-Saclay, DSM, IRFU, SAp, F-91191 Gif-sur-Yvette, France.

L. Soderblom, U.S. Geological Survey, 2255 North Gemini Dr., Flagstaff, AZ 86001, USA.